Remote Sensing of Environment 211 (2018) 167–183

Contents lists available at ScienceDirect

Remote Sensing of Environment

journal homepage: www.elsevier.com/locate/rse

Quantification of selective logging in tropical forest with spaceborne SAR interferometry

Yang Lei[a,*], Robert Treuhaft[a], Michael Keller[a,b], Maiza dos-Santos[b], Fabio Gonçalves[c], Maxim Neumann[d]

[a] Jet Propulsion Laboratory, California Institute of Technology, 4800 Oak Grove Drive, Pasadena, CA 91109, United States
[b] USDA Forest Service, International Institute of Tropical Forestry, Rio Piedras, Puerto Rico, EMBRAPA Agriculture Informatics, Campinas, SP, Brazil
[c] Canopy Remote Sensing Solutions, Florianopolis, SC, Brazil
[d] Google Cloud AI, Sunnyvale, CA 94089, United States

ARTICLE INFO

Keywords:
Spaceborne InSAR
Tropical selective logging
Fire
Forest disturbance
TanDEM-X
ALOS-2

ABSTRACT

Tropical forest disturbance (such as selective logging and fire) along with deforestation have significant contributions to the carbon source due to land-use change and anthropogenic CO_2 emissions, and thus envisioned by United Nation's REDD+ programme. In previous work, spaceborne single-pass InSAR phase-center height has been shown to have the capability of accurately monitoring the subtle height change due to forest growth and degradation (with meter or even sub-meter level RMSE about the regression curve fit to time). In this paper, a new approach using spaceborne SAR interferometry has been developed to detect and quantify selective logging events. In particular, a quantitative indicator of forest disturbance is first defined, namely disturbance index (DI; from 0 "no disturbance" to 1 "deforestation"). A numerical field data-based InSAR simulation is then performed to study the functional relationship between the field-measured DI and InSAR relative phase-center height change from a modeled perspective. A selective logging event (October 2015 through January 2016) over the Tapajos National Forest in Brazil is used for experimental validation. The InSAR-inverted DI estimates derived from DLR's TanDEM-X time-series data were compared with those measured from a field work over 32 quarter-hectare stands at Tapajos with relative RMSE of 30% for DI up to 0.3 and the disturbance epoch can be determined with an average accuracy of 13 days (constrained by the satellite repeat interval usually on the order of 2 weeks). As a comparison, the repeat-pass InSAR coherences from the concurrent JAXA's ALOS-2 data are shown to qualitatively correspond to the TanDEM-X results, confirming both the location and the epoch of the disturbance event. This new method is anticipated to contribute to the range of tools being developed for large-scale forest disturbance assessment and monitoring (for UN's REDD+ programme) through using spaceborne single-pass InSAR missions (e.g., DLR's TanDEM-X and in the future, TanDEM-L).

1. Introduction

Recent studies have shown that there is a net source of 1.3 ± 0.7 Pg-C y^{-1} resulting from the offsetting effects of tropical deforestation emission and the regrowth of secondary forests (Pan et al., 2011). In addition, tropical forests may be taking up 1.4 ± 0.4 Pg-C y^{-1} caused by CO_2 fertilization effects (Schimel et al., 2015). However, these budgets do not account for changes due to selective logging in the tropics that also lead to immediate carbon losses and later gains as forests recover biomass over decades (Rutishauser et al., 2015). It has been increasingly noticed that selective logging, although only occurring over limited area and short periods of time, can have a considerable net effect that is even comparable to deforestation when considering a larger scale over a longer period. Due to the small changes (and thus difficult to detect) in remote sensing imagery, few techniques have been reported to be capable of robustly and accurately measuring selective logging with sufficient spatial and temporal resolution in the literature. While selective logging may be identified using passive optical remote sensing techniques from satellites, the same techniques have limited sensitivity to carbon stock changes (Stone and Lefebvre, 1998; Souza and Barreto, 2000; Asner et al., 2002; Souza et al., 2003; Keller et al., 2004; Asner et al., 2005; Asner et al., 2009). Multi-temporal airborne lidar remote sensing can effectively quantify the change in carbon stocks from selective logging (Andersen et al.,

* Corresponding author.
E-mail addresses: leiyangfrancis@gmail.com (Y. Lei), robert.n.treuhaft@jpl.nasa.gov (R. Treuhaft), mkeller.co2@gmail.com (M. Keller), maizanara@gmail.com (M. dos-Santos), fabio@canopyrss.tech (F. Gonçalves), neumann.maxim@gmail.com (M. Neumann).

https://doi.org/10.1016/j.rse.2018.04.009
Received 8 December 2017; Received in revised form 20 March 2018; Accepted 5 April 2018
Available online 24 April 2018

2014; Silva et al., 2017) but it is relatively expensive to implement. Cost-effective options are needed to respond to the United Nations Framework Convention on Climate Change (UNFCCC) initiative for Reducing Emissions from Deforestation and forest Degradation (REDD +; Houghton et al., 2010). Understanding forest structural changes also support efforts aimed at quantifying biodiversity, particularly given the rapid declines and losses of many plant and animal species worldwide (Potapov et al., 2008).

Among the various types of sensors, a spaceborne InSAR system has the potential of mapping forest biomass and height as well as detecting forest disturbance within the world's forested biomes and on a monthly to weekly frequency regardless of day or night (Rosen et al., 2000). A single-pass InSAR system (such as NASA's SRTM mission (Farr et al., 2007) and DLR's TanDEM-X mission (Krieger et al., 2007)) is able to measure the interferometric phase accurately without much contamination by the atmosphere and/or the temporal change of the targets. Successful forest height inversion along with estimation of other parameters (e.g. biomass, forest density) using various techniques such as Polarimetric InSAR (PolInSAR) have been widely reported (Cloude et al., 2013; Askne et al., 2013; Kugler et al., 2014; Sadeghi et al., 2014; Lee and Fatoyinbo, 2015; Treuhaft et al., 2015; Qi and Dubayah, 2016). However, due to the assumptions made for the InSAR and PolInSAR scattering model, e.g. the widely-adopted Random Volume over Ground (RVoG) model (Treuhaft and Siqueira, 2000; Papathanassiou and Cloude, 2001), the error of the forest height estimates is usually on the order of several meters with a forest stand size of hectares, and may be prone to even larger uncertainty and bias over the tropical forest (Kugler et al., 2014).

Rather than using InSAR model-inverted height, in this work we use a model-free approach to measure the original InSAR phase-center (mean) height change with high accuracy, which further allows the estimation of the amount and epoch of forest disturbance. It is this accurate measurement of phase-center height that enables the creation of Digital Elevation Model (DEM) products from spaceborne single-pass InSAR missions (e.g. SRTM and TanDEM-X). In previous work (Treuhaft et al., 2017), it has been suggested that this phase-center height monitors forest height and biomass change with meter- (or even sub-meter) level RMSE over quarter-hectare stands by using a time series of TanDEM-X InSAR phase observations. Here, this approach will be adapted and automated (for most of the steps) to monitor a selective logging event using TanDEM-X data. In fact, single-pass InSAR phase-center height has been used previously to monitor forest biomass, height and stem volume (Solberg et al., 2013a; Fatoyinbo and Simard, 2013; Askne et al., 2017). These studies, however, focused primarily on estimation of these biophysical parameters at individual epochs as opposed to the time-series analysis. InSAR phase-center height has also been reported to detect forest clear-cuts (Solberg et al., 2013b; Solberg et al., 2014), but it was based on an 11-year net change of forest height between SRTM-X (2000) and TanDEM-X (2011) rather than a dense times-series analysis with one single sensor.

The paper is structured as follows. Section 2 describes the study area and the available data, ground and satellite data. Section 3 describes the forest disturbance detection approach using spaceborne single-pass InSAR. The experimental validation results are detailed in Section 4. Section 5 contains a brief discussion and conclusions.

2. Study area and experimental data

The study focused on a small area (~1700 ha) where reduced impact selective logging operations took place in late 2015 through early 2016 in the Tapajos National Forest (S 3°22′, W 55°00′) south of Santarem, Para in the Brazilian Amazon region (Fig. 1). The region of tropical moist forest receives about 2000 mm of precipitation per year and has an annual mean temperature of 25 °C (Silver et al., 2000). The logging area studied is sited on a mainly flat plateau with well-drained soils predominantly clay-textured Oxisols sand-loam-textured Ultisols (60% sand, 38% clay, 2% silt) (Silver et al., 2000). Vegetation at the site is evergreen or semi-deciduous with a total aboveground live biomass (dry weight) of about 282 Mg ha^{-1} (Keller et al., 2001).

Logging was conducted using reduced impact techniques. This involves planning the location of roads, log decks and skid trails and the use of directional felling to minimize collateral damage to the forest (Holmes et al., 2002). Common timber species in the region are *Manilkara huberi*, *Carapa guianensis*, *Couratari guianensis*, *Licaria brasiliensis*, and *Nectandra rubra*. Diameter cutting limits vary by species but generally only trees > 55 cm diameter at breast height (DBH) were felled. This logging strategy, that bigger trees are felled first, is termed the "top-down" concept in this work and will be used later in Section 3 for modeling the InSAR responses. Please note that although the "top-down" logging strategy is adopted in the current field campaign, it is not always the logging protocol. Sometimes, the most valuable hardwoods (that are not necessarily the tallest) are removed. In future work, various scenarios for the characteristics of the trees removed should be analyzed and modeled.

We established 32 inventory plots (50 × 50 m) in the Anambé Project community managed logging area (Fig. 1) in the forest managed by the Brazilian Chico Mendes Institute for Biodiversity (ICMBio). Inventory plots were surveyed approximately one month prior to the start of logging operations and then again within three months of the end of logging. For the initial inventory, all trees with DBH ≥10 cm were accounted for and measured within the plot area. Species were identified by an experienced para-taxonomist. Following logging, a second survey identified logging damage accounting for trees felled and those killed or damaged by logging activities. Tree-by-tree summaries were recorded including the species, DBH, the dates of logging (both felling and skidding processes), as well as the condition of logging (both position and cause), while the plot-level disturbance record will be shown later in Section 4.

In coordination with DLR, six TanDEM-X bistatic InSAR pairs (Table 1) with the format of Coregistered Single look Slant range Complex (CoSSC) were available over this logging period, i.e., three of them in ascending mode (20151030, 20151121, 20151202) and the other three in descending mode (20151129, 20151210, 20160123). The Height of Ambiguity (HoA; the amount of height change that leads to a 2π change in interferometric phase; Rosen et al., 2000) was between 60 m and 70 m with the interferometric vertical wavenumber κ_z around 0.1 rad/m.

As a cross-validation, through coordinating with JAXA, six concurrent ALOS-2 Level 1.1 FBD (fine beam dual-polarization) SAR acquisitions (Table 2) were obtained (20150920, 20151018, 20151101, 20151227, 20160110, 20160207), while only four interferometric pairs out of the possible combinations have relatively high InSAR scene-wide mean correlation magnitude (between 0.1 and 0.4 after calibration) despite the generally dry conditions throughout the acquisition period. The interferometric vertical wavenumber κ_z is very small (< 0.01 rad/m) with the HoA > 500 m.

Both of the HH-pol TanDEM-X CoSSC and ALOS-2 Level 1.1 data in this work were processed using NASA JPL's ISCE software (Rosen et al., 2012) and projected onto the SRTM DEM with a spatial resolution of 30 × 30 m. The window size (number of pixels in range and azimuth) of correlation estimation is 36 × 22 for TanDEM-X (ground resolution of 50 × 50 m), and 4 × 8 for ALOS-2 (ground resolution of 30 × 30 m).

3. Analytical methods

In this section, we first define a quantitative metric of forest disturbance, and then describe a new forest disturbance detection approach using spaceborne single-pass SAR interferometry along with a coherent electromagnetic InSAR scattering model, which connect the InSAR observable to the disturbance metric.

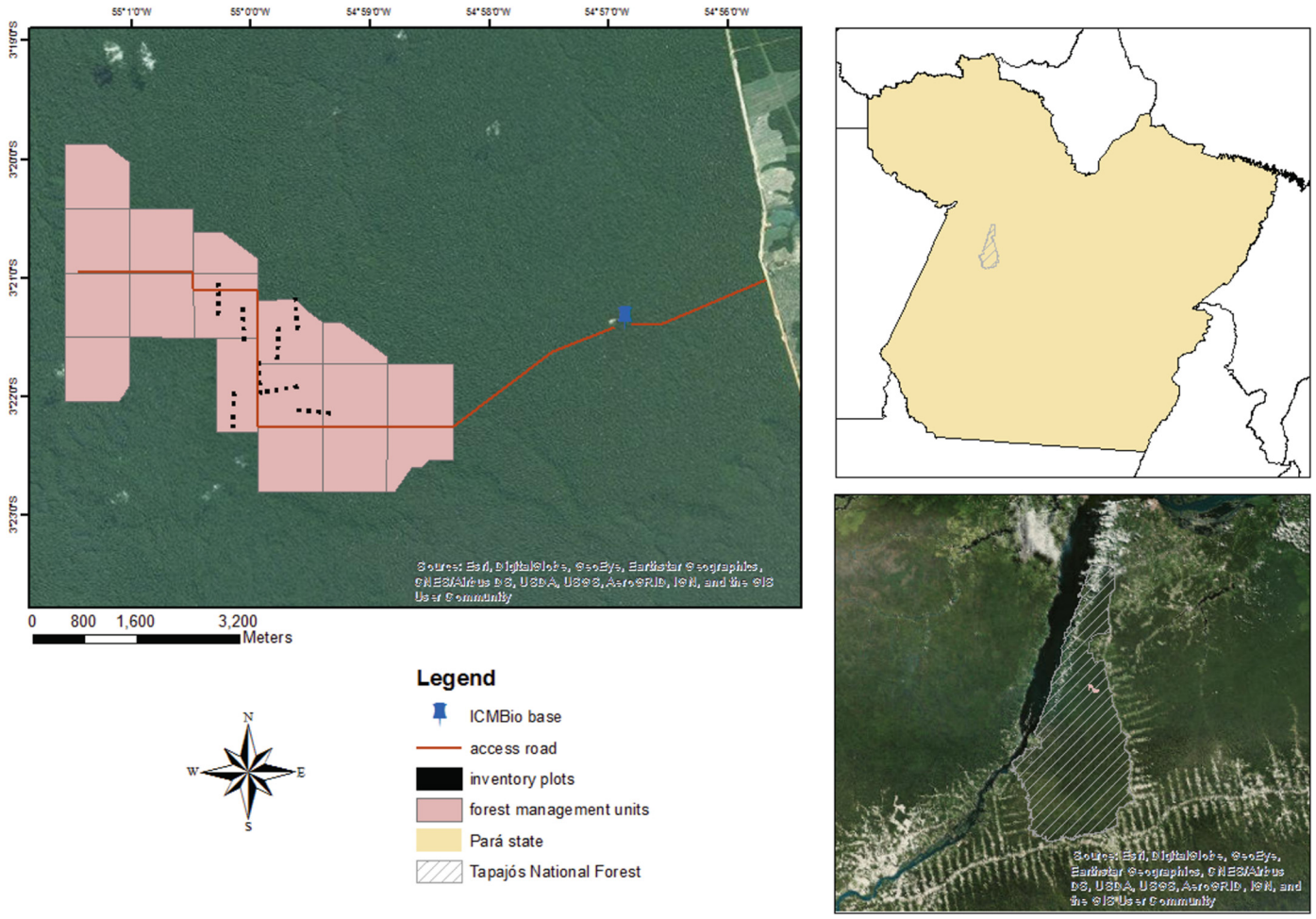

Fig. 1. Selective logging area at Tapajos National Forest in central Brazilian Amazon, overlaid on top of the optical image. Field measurements were recorded over the 32 quarter-hectare plots ("black" dots). The "top left" panel represents the small "pink" area in the "bottom right" subplot, where the "grey shaded" region corresponds to the smaller one in the "top right" subplot. In the "top left" panel, the "blue" pin marks the Instituto Chico Mendes de Conservação da Biodiversidade (ICMBio) base along the logging access road ("red" line). (For interpretation of the references to color in this figure legend, the reader is referred to the web version of this article.)

3.1. Disturbance index

The amount of forest structural disturbance (in the case of felling or removal) relates to the disturbed tree crown projected area per resolution area (Pereira et al., 2002), which can also be related to the leaf area-based optical disturbance index (Schmidt et al., 2015). This assumption enables us to define a crown area-based measure of forest disturbance and further to characterize the disturbance signature in the InSAR measurements as a function of this disturbance metric.

We define an area-based measure of forest disturbance, i.e., Disturbance Index (DI; denoted as *DI*), as

Table 2
ALOS-2 InSAR data. All of these InSAR pairs are fine-beam dual-pol (FBD) images with both HH and HV polarization (only the HH-pol data is used in this work), incidence angle of 28.2°, ascending orbit direction. Calculation of the averaged forest temporal coherence will be discussed in Section 4.4.

Acquisition dates	κ_z (rad/m)	Scene-wide mean coherence	Averaged forest temporal coherence
20150920–20151018	0.0034	0.1866	0.2015
20151018–20151227	0.0024	0.1464	0.1785
20151227–20160110	0.0079	0.3433	0.4941
20151227–20160207	0.0033	0.1294	0.1264

Table 1
TanDEM-X InSAR data. All of these InSAR pairs have an incidence angle of 41°, and only HH-pol data is used in this work. "TSX" and "TDX" refer to TerraSAR-X and TanDEM-X, respectively.

Acquisition date	Orbit direction	HoA (m)	κ_z (rad/m)	Polarizations	Bandwidth (MHz)	Master satellite
20151030	Ascending	70.97	0.0893	HH, VV	150	TSX
20151121	Ascending	63.27	0.1002	HH, VV	150	TDX
20151129	Descending	71.91	0.0885	HH	100	TDX
20151202	Ascending	64.91	0.0976	HH, VV	150	TSX
20151210	Descending	71.41	0.0886	HH, VV	150	TDX
20160123	Descending	65.4	0.0967	HH, VV	150	TSX

$$DI = \frac{A_d}{A_{ud} + A_d} = \frac{A_d}{A_t} \quad (1)$$

where A_d and A_{ud} are the total disturbed and undisturbed tree crown (projected) area within the plot, and $A_t = A_{ud} + A_d$ is the total tree crown area of the plot. By definition, DI is a value that continuously goes from 0 to 1, where $DI = 0$ means no disturbance, and $DI = 1$ means deforestation. Note that tropical forests have multi-layer canopies so that removal of a tall tree does not necessarily result in bare ground below, in which case the dependence of DI on the cutoff diameter for plot survey may need to be investigated in the future as a sensitivity test for better fits.

According to a previous study in the same study site (Gonçalves, 2014), tree crown radius C_R (in meters) tend to scale linearly with the square root of DBH (denoted as D; in cm), i.e., $C_R = \beta_0 + \beta_1\sqrt{D}$ with β_0 and β_1 being linear regression coefficients. Therefore, the crown (projected) area C_A can be estimated as

$$C_A = \pi C_R^2 = \pi(\beta_0 + \beta_1\sqrt{D})^2 \approx a + b\bullet D \quad (2)$$

where a linear fit with coefficients a and b (ignoring the square root term without noticeable difference) is found to correspond reasonably well with the previous in-situ measurements of (Gonçalves, 2014). The coefficients a and b for primary forests at Tapajos are estimated as: $a = -2.79\ \mathrm{m}^2$ and $b = 1.53\ \mathrm{m}^2\,\mathrm{cm}^{-1}$. Equating the right-hand side of Eq. (2) to zero gives the validity range of Eq. (2) as $D > 1.82$ cm, which is well below the DBH cutoff of 10 cm used in the field measurements.

Substituting Eq. (2) into Eq. (1) and summing over all of the trees in the plot, we have

$$DI = \frac{\sum_{n_d=1}^{N_d} C_A^{(n_d)}}{\sum_{n_t=1}^{N_t} C_A^{(n_t)}} = \frac{\sum_{n_d=1}^{N_d}(a + b\bullet D^{(n_d)})}{\sum_{n_t=1}^{N_t}(a + b\bullet D^{(n_t)})} = \frac{a\bullet N_d + b\bullet\sum_{n_d=1}^{N_d} D^{(n_d)}}{a\bullet N_t + b\bullet\sum_{n_t=1}^{N_t} D^{(n_t)}} \quad (3)$$

where N_d and N_t are the number of disturbed trees and total trees, respectively, while n_d and n_t are their corresponding summation indices. The superscript above is used to denote the crown area or DBH associated with each tree. Because DBH in units of cm is between 10 cm and 100 cm ($D^{(n_d)} \gg 1$), the D-related sums dominate, i.e., $\sum_{n_d=1}^{N_d} D^{(n_d)} \gg \sum_{n_d=1}^{N_d} 1 = N_d$. Given the similar order of magnitude for coefficients a and b, Eq. (3) can thus be simplified as

$$DI \approx \frac{b\bullet\sum_{n_d=1}^{N_d} D^{(n_d)}}{b\bullet\sum_{n_t=1}^{N_t} D^{(n_t)}} = \frac{\sum_{n_d=1}^{N_d} D^{(n_d)}}{\sum_{n_t=1}^{N_t} D^{(n_t)}} \quad (4)$$

Using the summed field measurements of DBH thus provides a simple and practical damage estimate (DI). It should be noted that depending on the concrete forest species and management, the crown radius-DBH relationship could be complicated with the coefficients on different order of magnitude, where Eq. (3) (or its modified form) needs to be directly used instead of Eq. (4). If there is no simple relationship between crown radius and DBH, the direct crown area measurements (if available) or the proper allometric equation of crown radius can also be used by following the same procedure in deriving DI.

Also, the DI estimate here is defined based on the two-dimensional crown area. Although the change of crown area also implicitly relates to the change of forest height and/or InSAR phase height in the vertical dimension (as shown later), an alternative solution is to directly define a DI metric based on the forest vertical characteristics (e.g. height metrics). Since the tree-by-tree height metrics are not available from the current field work, in this study, we only adopt the crown area-based DI definition leaving the height-based DI definition to be evaluated in future work.

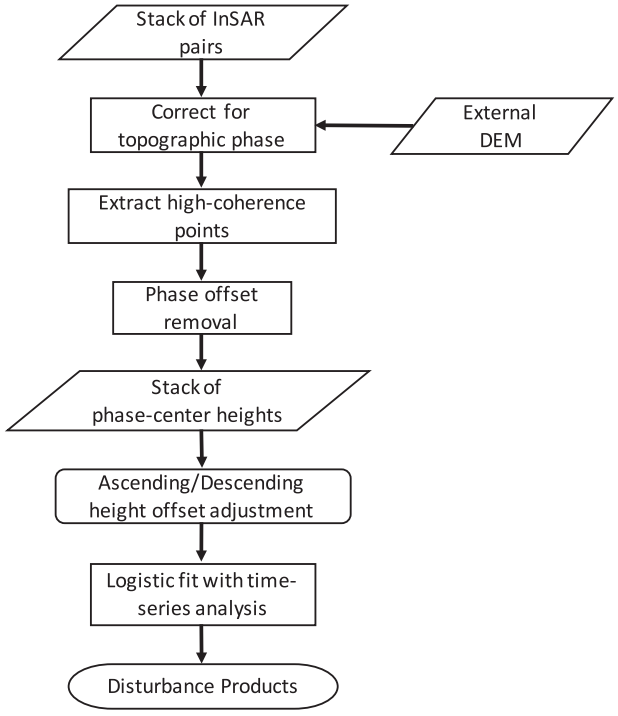

Fig. 2. Flowchart of InSAR data processing for the forest disturbance detection approach developed in this paper.

3.2. Forest disturbance detection approach using single-pass InSAR phase

Because spaceborne single-pass SAR interferometry has the capability of measuring the interferometric phase (and thus phase-center height) accurately, it is possible to monitor the change of phase-center height as a function of time. In previous work (Treuhaft et al., 2017), time-series of phase-center height from TanDEM-X data were used to monitor forest growth and/or degradation at meter- (or even sub-meter) level over quarter-hectare forest stands in the same region. We adapt this approach to examine forest disturbance from selective logging by refining and automating some of the processing steps.

The processing flowchart of the single-pass InSAR approach is shown in Fig. 2, with the individual components described in detail below.

As a first step, the apparent InSAR phase must be flattened (termed *flat-earth removal*, and more precisely, to remove the range-dependent part of the interferometric phase) in order to reveal the signatures due to topography and forest structure as well as its change. In this study, we flattened the InSAR phase measurement with use of an external DEM (SRTM), which simplifies the following data processing and analysis. This is illustrated in Fig. 3a. Note that the DEM does not have to be that accurate in this type of study, because once the same trend of the topography is "flattened" (or removed), it is the relative change in the time series of the phase-center height that will be exploited to provide the disturbance information.

If the 30 m-resolution C-band SRTM DEM (SRTM, 2014) is used for phase flattening (both flat-earth and topographic phases are removed), the differential height between the TanDEM-X phase-center height and SRTM DEM height is not the real phase-center height; rather, it is the difference between the X-band ("blue" curve) and C-band ("red" curve) phase-center heights as seen in Fig. 3a. Also, it is expected that at each epoch the flattened InSAR phase has a random offset due to atmospheric delay and/or system bias (Krieger et al., 2014), which will be removed later. Therefore, after phase flattening, the random offset at each epoch is first maintained and the resulting differential phase-center height is illustrated as the "green" curve in Fig. 3b.

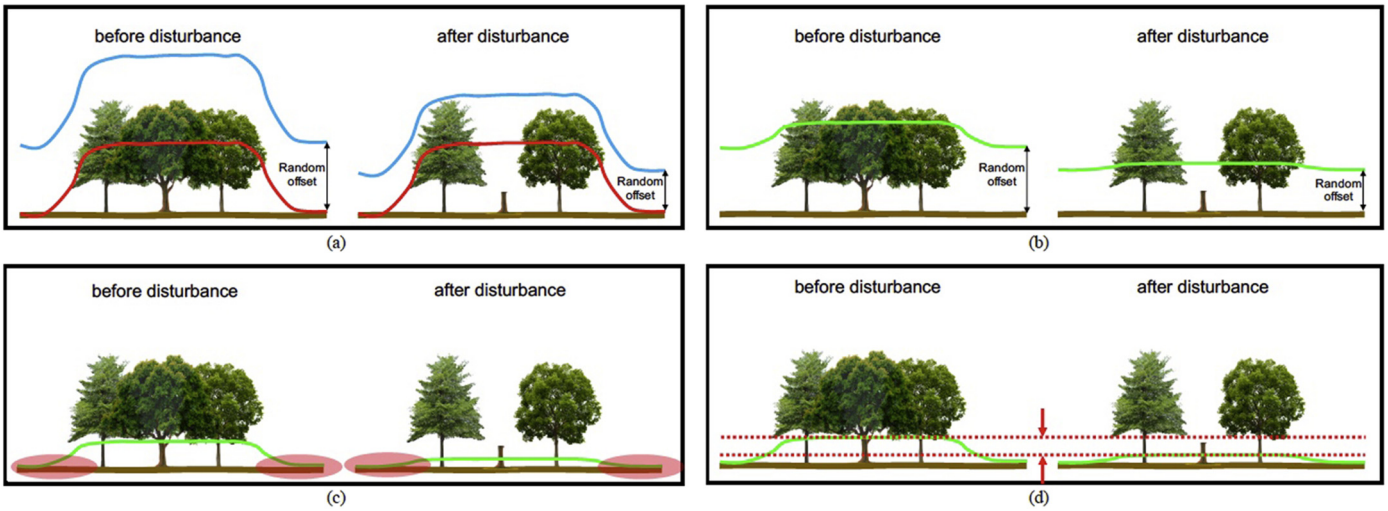

Fig. 3. Illustration of the TanDEM-X InSAR processing steps. (a) to (b) represents phase flattening, (b) to (c) refers to random phase removal, (c) to (d) is the time-series analysis. In (a), the "blue" curve is the TanDEM-X apparent phase center which includes random phase offset that can be different in different data acquisitions, and the "red" curve is the SRTM apparent phase center. In (b), the "green" curve is the relative phase-center height between TanDEM-X and SRTM. In (c), the "red" shaded area denotes the high-coherence points used for the offset removal. In (d), the "red" dotted lines indicate the phase-center height drop due to disturbance. (For interpretation of the references to color in this figure legend, the reader is referred to the web version of this article.)

Next, the InSAR phase measurements with high coherence are used to estimate and remove the random phase offset, similar to the Persistent Scatterer (PS) technique (Hooper et al., 2004). Here, at each epoch, the high-coherence points are identified via thresholding and mostly located over bare ground surfaces. Therefore, the mean InSAR phase of these high-coherence points will be subtracted from the entire InSAR phase image so that the average phase center of the high-coherence points always corresponds to zero height (as marked by the "red" shaded area in Fig. 3c) ignoring the topographic deformation within a short time period such as earthquakes. This treatment is convenient and useful because the high-coherence points mostly correspond to bare ground surfaces, buildings, roads, and other persistent scatterers, which have constant (or slowly varying) topography. Note there could be a phase bias at some high-coherence points where SRTM (2000) saw some canopy that was later cleared by the time of TanDEM-X (2015) revisited the area. However, after averaging over all of the high-coherence points within the TanDEM-X imagery, this effect is negligible unless the entire imagery is affected. Also, as mentioned earlier, if this effect along with other DEM error persist in the time series of InSAR imagery, they can be eventually cancelled out when studying the relative InSAR phase height change through differentiation. Although the same set of high-coherence points is desired for all TanDEM-X acquisitions, we applied this method for individual acquisitions and did not find any noticeable difference (possibly due to the similar HoA or κ_z). Hence, a dense time series of calibrated InSAR phase-center height can be achieved to indicate the height drop (specified by the "red" dotted lines in Fig. 3d) due to logging.

The above-mentioned procedure can be summarized as follows for the i^{th} epoch,

$$h^i = \frac{\phi^i - \phi^i_{topo} - \phi^i_{high}}{\kappa^i_z} \tag{5}$$

where h^i is the relative (calibrated) phase-center height between TanDEM-X and SRTM, ϕ^i is the apparent TanDEM-X InSAR phase, ${\phi_{topo}}^i$ is the topographic InSAR phase (simulated from SRTM DEM in this work thus also including the C-band phase center of vegetation), ${\phi_{high}}^i$ is the average flattened phase of the high-coherence points only, and ${\kappa_z}^i$ is the interferometric vertical wavenumber (phase-to-height conversion factor that is inherent to an InSAR system and its viewing geometry). Since ${\kappa_z}^i$ varies with the local incidence angle, it is a variable across the range direction even for flat terrain, and also can have a much larger dynamic range for complicated topography with large surface slopes. However, in this work, due to the narrow range swath width and relatively flat topography, the incidence angle varies by about 1° over the entire study area. Therefore, by using the scene-center incidence angle, the local incidence angle thus has an error of ± 0.5°, which is 0.001 rad/m (1% relative) for the resulting κ_z^i. Please note that, if a residual range and/or azimuth phase ramp (although not seen in this study) is resulted, one also need to remove the phase ramp through use of a two-dimensional curve fitting as in (Treuhaft et al., 2017).

Given a time series of calibrated InSAR phase-center height (as illustrated in Fig. 4), a sudden height drop will be induced by the forest disturbance event such as logging. We thus fit a generalized logistic function (Treuhaft et al., 2017), i.e.,

$$y = A + B \bullet x + \frac{C}{1 + e^{-D \bullet (x - E)}} \tag{6}$$

where y is the phase-center height at epoch x. The first two terms on the right-hand side ($A + B \cdot x$) model a linear height change trend over time (e.g. forest growth or degradation), and the third term represents an abrupt disturbance event (deforestation, selective logging and fire). The parameter C can be related to the amount of the height change during the disturbance, D describes the steepness of the height change, and E represents the epoch of the disturbance. Given the epoch of disturbance, E, the amount of change in the phase-center height can be calculated by taking the difference of the logistic function values before

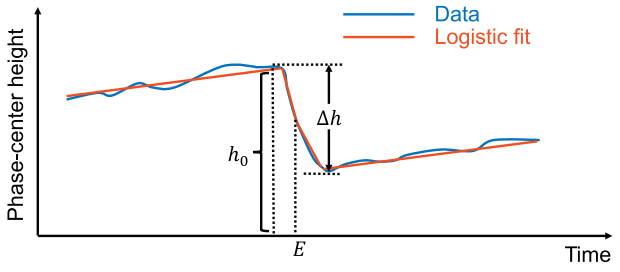

Fig. 4. Illustration of the times-series analysis by fitting a generalized logistic function ("red") to the time series data ("blue"). (For interpretation of the references to color in this figure legend, the reader is referred to the web version of this article.)

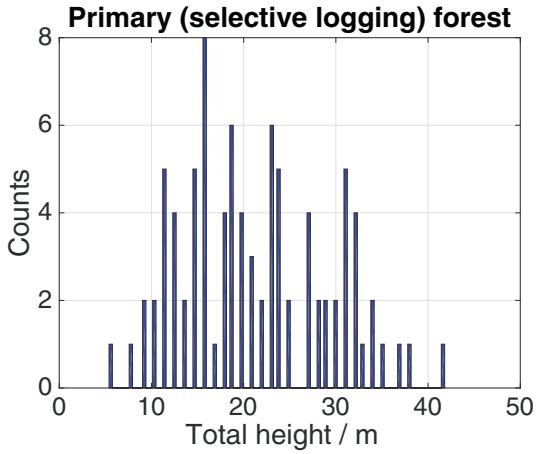

Fig. 5. Histogram of total tree height for a quarter-hectare primary (selective logging) forest at Tapajos.

and after the disturbance (as shown in Fig. 4), which is denoted as Δh (positive number; if $B \approx 0$ over a short time period, $\Delta h \approx |C|$). Suppose the absolute phase-center height before disturbance is h_0, a relative phase-center height drop is thus $\frac{\Delta h}{h_0}$.

3.3. Coherent electromagnetic modeling of InSAR phase-center height

In order to further relate this InSAR-measured relative phase height drop to the field-measured disturbance index (as defined in Eq. (1)), we simulated the electromagnetic scattering responses from a primary (also selectively logged) forest stand at Tapajos, where a comprehensive field record is available in (Treuhaft et al., 2015). In this work, the term "primary forest" refers to mature forest in this area in order to distinguish from "secondary forest" that is shorter and denser (Treuhaft et al., 2017). The histogram of the total height for trees in this quarter-hectare stand is illustrated in Fig. 5, where it can be seen that primary (mature) forest at Tapajos has large dynamic range (from 5 m to 40 m) with the mean value around 20 m.

In the simulation, each tree is represented with an ellipsoidal crown with the trunks ignored for X-band signals. The distributions of crown parameters (depth and radius) are specified by the field data. Further, the scattering responses of the ellipsoidal crowns and an underlying ground surface are computed by decomposing them into a mesh grid of point scatterers (particles), which is similar to (Solberg et al., 2010). This simplification will lose the polarization information; however, the scattering response of a point scatterer is computationally easy to calculate, so it is useful to study the effect of volume removal on InSAR phase height drop. As shown later, the extinction coefficient of primary forest stands in our study area is around 0.05 dB/m (in this work it represents the extinction sigma, not the vertical attenuation coefficient). Therefore, vertical attenuation layers with the initial extinction coefficient (denoted as $k_{e0} = 0.05$ dB/m) is included in the simulation. In addition, the initial ground-to-volume ratio (denoted by m_0; in dB) is specified to constrain the number of ground particles relative to that of the crown particles. Typical values of ground-to-volume ratio at X-band exists in the literature, for example in (Praks et al., 2007), it was reported that the ground-to-volume ratio for a 20-m tall boreal forest at X-band is between -100 dB to 0 dB with most of them below -10 dB. Therefore, it is reasonable to assume $m_0 \leq -10$ dB for our tropical primary forest.

Using TanDEM-X's viewing geometry, the simulation is performed over the above 50 × 50 m primary forest stand. Given TanDEM-X's range and azimuth resolution, hundreds of independent looks are generated so that multi-look averaging is used to approximate the ensemble-averaged InSAR phase-center height. As for the volume removal, we adopted the "top-down concept" that is to first remove the tallest trees and then gradually down to shorter trees. This is to mimic the realistic selective logging strategy as described in Section 2. Because the extinction coefficient is proportional to the number density (Treuhaft et al., 1996), the volume removal will effectively reduce the number density (and thus extinction coefficient) by a factor of *DI*. The number of ground scatterers is assumed to be fixed during this volume removal process. The actual *DI*'s are then calculated as the DBH-based ratio using Eq. (4). The scene of scatterers is illustrated in Fig. 6 for three *DI*'s, i.e., $DI = 0$, $DI = 0.5$, and $DI = 0.9$.

From the simulation, the quantitative comparison between the relative InSAR phase height drop $\frac{\Delta h}{h_0}$ and *DI* is shown in Fig. 7, where the initial ground-to-volume ratio m_0 varies from -∞ dB to 0 dB. For the no-ground scenario ($m_0 = -\infty$ dB), the simulated InSAR phase height is reported as $h_0 = 25$ m. The mean value at each "x" marker is calculated by repeating the simulations 100 times and taking the average while the error bar is not an indicator of the error of the mean but the standard deviation for a one-time simulation. Therefore, the error bar also implies the InSAR coherence level, i.e., a higher coherence corresponds to a smaller error bar.

From Fig. 7, it can be seen that in all cases, $\frac{\Delta h}{h_0}$ is a monotonically increasing function of *DI* although some deviation from the "1:1" line may occur depending on the ground scattering contribution (a best "1:1" fit is achieved for $m_0 = -15$ dB). This is probably because: there is a large height diversity as revealed from Fig. 5 and Fig. 6a, hence the "top-down" volume removal will effectively drop the InSAR phase height proportional to DI (or the change of total crown area).

Hence, it is the lateral heterogeneity (height diversity) of the primary forest along with the "top-down" volume removal concept that enable the InSAR phase height drop proportional to DI, which may not be easily revealed from a random (laterally homogeneous) volume

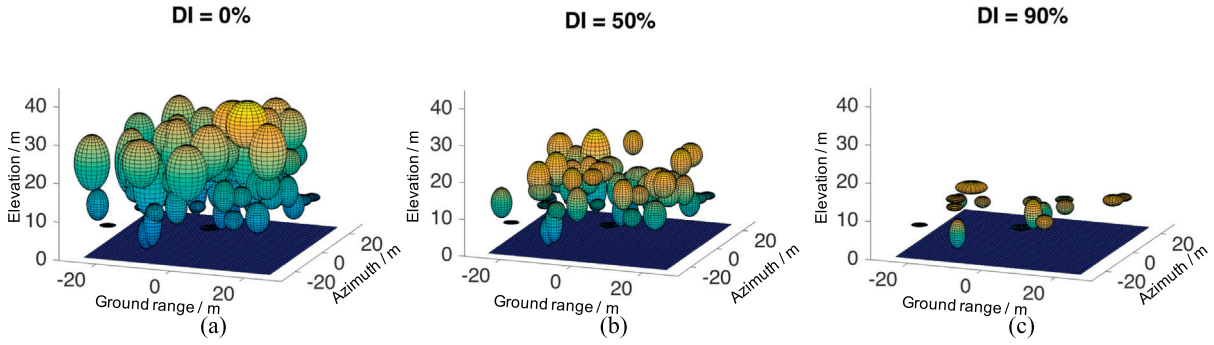

Fig. 6. Illustration of the scatterer scene for the primary (selective logging) forest with (a) DI = 0% (maximum height of 40 m), (b) DI = 50% (maximum height of 20 m) and (c) DI = 90% (maximum height of 10 m). Tree crowns are shown as ellipsoids and the underlying planar surface represents the ground layer under the canopy. Both the ellipsoids and planar surface are further decomposed into a mesh grid of point scatterers. The crown parameters (depth and radius) are extracted from field data.

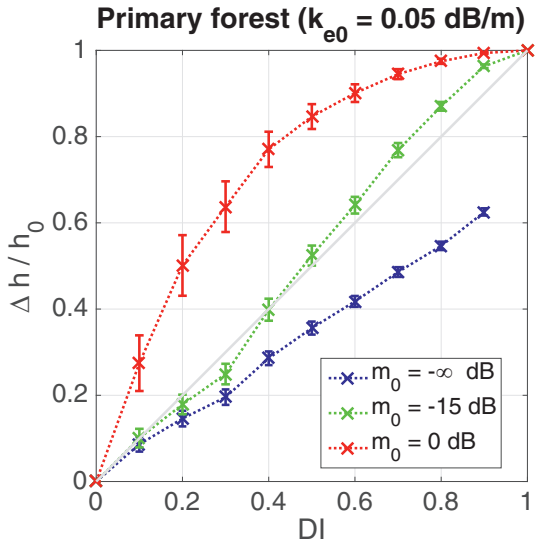

Fig. 7. Quantitative simulation results of the functional relationship between the relative InSAR phase height drop ($\frac{\Delta h}{h_0}$) and DI for the primary (selective logging) forest. Initial extinction coefficient (k_{e0}) is 0.05 dB/m, and initial ground-to-volume power ratio (m_0) is set to -∞ dB, −15 dB and 0 dB, respectively. TanDEM-X viewing geometry is used in the simulation. The "x" markers represent the mean values after repeating the simulation 100 times while the error bar is the standard deviation calculated from those 100-time simulations (i.e., error for 1-time simulation) not the error of the mean. (For interpretation of the references to color in this figure legend, the reader is referred to the web version of this article.)

model and/or vertical column removal concept. In fact, a uniform volume with zero extinction and no ground will have its InSAR phase height invariant to vertical column removal.

Also shown in Fig. 7 is the $m_0 = 0$ dB scenario, where the ground scattering becomes as large as volume scattering so that the InSAR phase center will be much closer to the ground and also approach the ground much faster after logging (with ground scattering enhanced due to less extinction effect). This is particularly related to lower-frequency scenarios, such as L-band, where the radar wave penetrates deeper resulting in a much larger ground-to-volume ratio.

The coherent scattering model (e.g. Fig. 7) provides a family of curves $\frac{\Delta h}{h_0}$ versus *DI*. To use this model in practice, one has to know the specific type of forest (with the comprehensive field measurements of forest characteristics) as well as the ground-to-volume ratio for the radar frequency used. As a result, a modeled "$\frac{\Delta h}{h_0}$ - *DI*" curve from the family can be generated to predict and/or fit to the measured InSAR phase height drop due to selective logging. As for the estimation of ground-to-volume ratio, an InSAR system equipped with full-pol capability can be exploited through using the PolInSAR technique (Papathanassiou and Cloude, 2001; Cloude, 2010).

In the above modeling analysis, the InSAR coherence was also examined. Since coherence is affected by the combination of two factors during the selective logging process, i.e., the decrease of extinction effect (that may either increase or decrease the coherence depending on the amount of ground scattering contribution), and the decrease of the top tree height (that increases the coherence), the overall trend of the InSAR coherence as a function of DI could be complicated depending more heavily on the level of ground contribution and particulars of the forest than the InSAR phase height, although coherence is indeed sensitive to and could be used to retrieve DI after some rigorous treatment. The complete analysis of the DI retrieval using InSAR coherence is beyond the scope of this paper and should be treated in the future.

An analytical solution with the use of the modified RVoG model was also tested. A major assumption in the classic RVoG model is the lateral homogeneity (and usually vertical homogeneity as well) within the volume (Treuhaft and Siqueira, 2000). Therefore, if the "top-down" removal concept is desired, the lateral heterogeneity and the associated DI definition (Eq. (1) and/or Eq. (4)) cannot be directly modeled. Instead, if the vertical column removal concept is considered, the DI definition can be used but the lateral heterogeneity is still not modeled so that the volume removal has very limited effect on the phase height drop for the reasons mentioned above. However, further considering 1) the decrease of top tree height or 2) the increase of ground scattering power during the volume removal has the potential to eventually bring the RVoG-modeled $\frac{\Delta h}{h_0}$ - *DI* relationship close to the numerical solution, where the latter is similar to varying the area-fill parameter in the Interferometric Water Cloud Model (IWCM) as shown in (Askne et al., 2013; Askne et al., 2017).

As will be shown in Section 4, by using the field data in this work, the following hypothetic relationship is considered for simplicity as the "green" curve in Fig. 7, i.e.,

$$\frac{\Delta h}{h_0} \approx DI. \tag{7}$$

which will be later validated with the experimental results.

As seen from Eq. (7), this approach not only requires the accurate measurements of InSAR phase height change Δh, but also an estimate of the totoal phase height h_0, which is usually less accurate than the phase height change. Here, we briefly summarize a few options for obtaining h_0 with the technical details provided in Section 4.2:

a) Lidar Digital Topography Model (DTM);
b) Polarimetric SAR Interferometry (PolInSAR);
c) A local constant through use of clear-cut stands;
d) Few-look InSAR phase;
e) SAR tomography.

Also, as mentioned in Section 2, if an alternative definition of DI that relates to forest height change is considered rather than the current crown area-based DI definition, InSAR phase height change Δh can be directly used without the need of estimating the total phase height h_0. This is worth further examination in future work. However, the current relative phase height drop (Eq. (7)) has its own merit since it is a physical measure for the percentage of biomass loss due to disturbance, which can be used to compare the carbon loss at various levels of biomass. In other words, a common InSAR phase height drop could induce essentially different amount of biomass loss depending on their pre-logging biomass level (Treuhaft et al., 2017).

4. Results

4.1. Time-series of relative InSAR phase-center height

The TanDEM-X InSAR phase was flattened through use of SRTM DEM (with both flat-earth and topographic phases removed). Because SRTM DEM is not a perfect DEM (i.e., C-band phase-center height is not zero over forests), the resulting phase-converted height is only a relative phase-center height (i.e., X-band phase-center height minus C-band phase-center height). The random phase offset was then removed by using the high-coherence points, which were selected with a scene-specific threshold of InSAR coherence (the scene-wide mean coherence plus one standard deviation) in this work. Because the ascending- and descending-mode imageries have different viewing geometry, the phase-converted heights have a slight offset (that are on the order of the TanDEM-X time-series RMSE), which were also removed by using their high-coherence points. The relative phase-center heights for the six HH-pol TanDEM-X InSAR pairs are illustrated in Fig. 8 (before removing the ascending/descending offset).

It can be seen that the "hot" spots (that appear in "orange" and

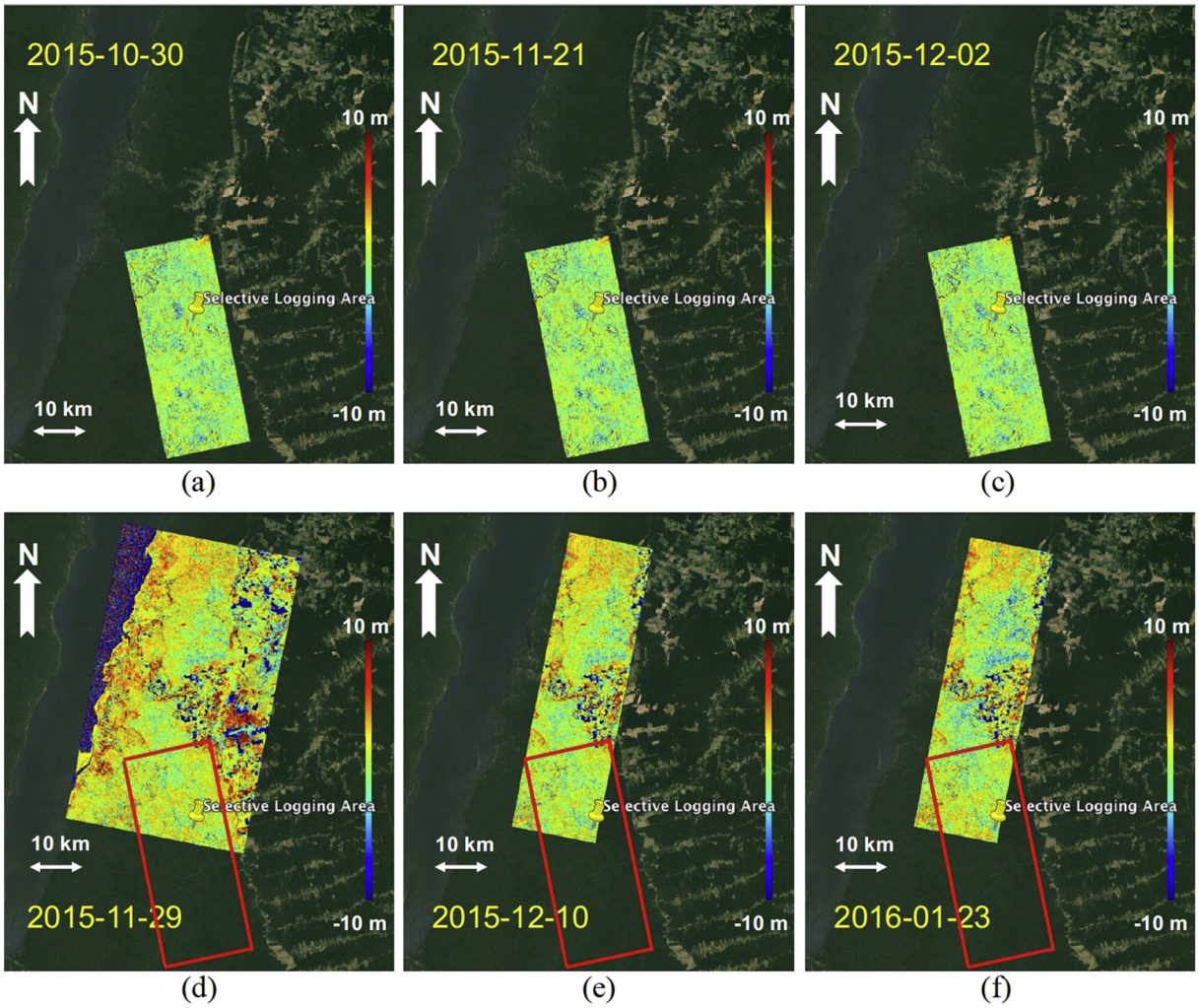

Fig. 8. HH-pol TanDEM-X InSAR phase-center heights (relative to SRTM DEM) over the Tapajos test site. The color scale is −10 m to 10 m as indicated. The "red" rectangles in the descending images (bottom panel) represent the boundaries of the ascending images (top panel). (For interpretation of the references to color in this figure legend, the reader is referred to the web version of this article.)

"red") reveal the increase of TanDEM-X phase-center height compared to SRTM's (possibly due to forest growth and building rise), while the "cool" spots (that appear in "blue") represent the decrease of phase-center height between TanDEM-X and SRTM (possibly due to logging considering the 15-year difference of their acquisition epochs). However, during a short time period, the phase-center height is very consistent as observed from these six epochs in October 2015 through January 2016 (the "red" rectangle in the descending imagery represents the boundary of the ascending imagery), except of the slight offset between ascending- and descending-mode imageries (that is maintained in Fig. 8). The apparent height offset between the ascending acquisition 20151121 and the descending one 20151129 is 1.5 m, which was used to further calibrate the two modes of images.

By sequentially taking the same-mode differential heights from Fig. 8, four pairs of differential phase-center height are obtained and illustrated in Fig. 9, with the top two corresponding to the ascending mode and the bottom two corresponding to the descending mode (where the "red" rectangle also outlines the boundary of the ascending imagery). The "red" dots outside the selective logging area represent those concurrent forest fire locations as observed by NASA's MODIS (Giglio et al., 2016), where it can be seen that the TanDEM-X phase-center height also has some corresponding drops. These results indicate that selective logging and/or fire (that appear as "dark" areas) can be detected from the TanDEM-X InSAR imagery (40 × 16 km), and also from the blowups of Fig. 9 it can be seen that different logging locations can be extracted at various epochs (i.e., selective logging moved from northwest to southeast as confirmed from field work) with the use of a dense time series of TanDEM-X images.

Next, the time series of the TanDEM-X phase-center height are illustrated in Fig. 10 for the 32 quarter-hectare plots, where the generalized logistic function (Eq. (6)) is fit to the InSAR time-series data with the parameters determined through a standard non-linear least-squares fit. The error bars are included due to the phase observational error given the measured InSAR coherence level (Treuhaft et al., 2017), however the reduced chi-squared metric is not used here because of few observations (only six points in this work). The detected phase-center height drop Δh along with its error (estimated by Monte Carlo simulations as described on Fig. 13) is shown for each plot, where a minus sign indicates height drop and a positive number represents a "false" increase due to random observational error. As observed from time-series analysis of TanDEM-X phase-center height over the normal forests in this study area (Treuhaft et al., 2017), the height estimation RMSE is on the order of 1–2 m (sometimes even less than a meter). Therefore, for a plot (such as "Plot 24") where there is a height increase/drop on the order of the RMSE, this may be due to the measurement uncertainty; however, if the drop is well beyond the RMSE (such as "Plot 6"), it is very possible that a real logging event occurred. Based on the error estimates in Fig. 10, it can be seen that most of the height change detections are statistically significant.

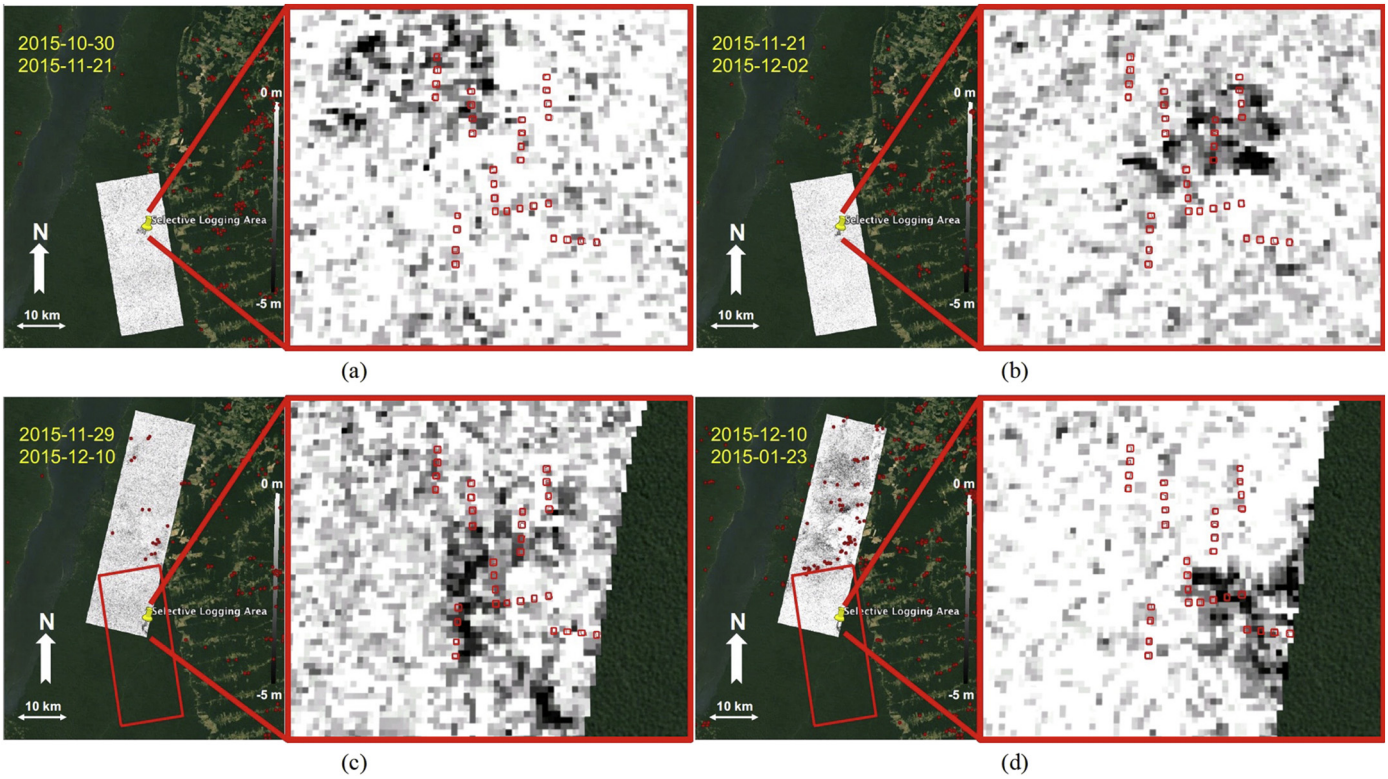

Fig. 9. TanDEM-X differential phase-center height, which correspond to the sequential change of the phase height images in Fig. 8 with the same mode of orbit direction. The pair of dates used for differentiation is indicated, as well as the grey scale (−5 m to 0 m). The closeup subfigures are shown over the 32 selective logging plots ("red" squares). The "red" rectangles in the descending images (bottom panel) are the boundaries of the ascending images (top panel) and the "red" dots outside the selective logging area represent concurrent fire locations from MODIS. (For interpretation of the references to color in this figure legend, the reader is referred to the web version of this article.)

4.2. Estimation of absolute InSAR phase-center height

In order to use Eq. (7) to calculate the TanDEM-X-measured DI metric, the absolute phase-center height h_0 must be determined, which in turn translates to an accurate measurement of the ground topographic phase. As discussed in (Treuhaft et al., 2017), InSAR phase-center height is approximately the backscatter power-weighted height not the total tree height. As enumerated in Section 3.3, below we discuss the technical details of these choices for h_0-estimation.

4.2.1. Using Lidar Digital Topography Model (DTM)

Previous studies have shown that using PolInSAR techniques for TanDEM-X data are capable of estimating the forest height along with the underlying topography with few-meter height estimation RMSE over boreal and temperate forests, however a little larger over tropics due to the complexity of the forest structure and small penetration depth at X-band (Kugler et al., 2014). Although it can be improved by incorporating the lidar-measured Digital Topography Model (DTM) data, this study determines height and height changes while the DTM data are not available. Note, if a lidar DTM is given, the absolute phase-center height can be immediately obtained without the use of any model-based inversion (e.g. PolInSAR) techniques, which is relevant to combining spaceborne single-pass InSAR and lidar missions (e.g., TanDEM-X and GEDI).

4.2.2. Using Polarimetric SAR Interferometry (PolInSAR)

We also examined the polarimetric diversity (PolInSAR complex-domain analysis) using the dual-pol (HH and VV) TanDEM-X measurements. In particular, the 2 × 2 dual-pol PolInSAR matrix was optimized by using the Schur decomposition theorem to depict the InSAR complex coherence region, and the underlying topographic phase was then determined with the standard PolInSAR line fit intersecting the unit circle in the complex domain (Cloude, 2010; Cloude et al., 2013; Kugler et al., 2014; Lee and Fatoyinbo, 2015).

As illustrated in Fig. 11, the analysis is performed for one bare field, one secondary forest (~20 m tall) and one primary forest (~40 m tall) in the surrounding regions of the current study area, where field-measured height estimates exist (Treuhaft et al., 2015). Here, we used one TanDEM-X test dataset (20140915) with HoA of 133 m from our previous work (Treuhaft et al., 2017). For each target, the co-polarized (HH and VV) InSAR complex coherence points, the two Schur-optimized coherences along with the two candidate ground points on the unit circle are expected to line up in the complex domain. It is the angular separation between the two optimized coherences that indicates the polarization diversity, which will be utilized to isolate (and thus retrieve) the forest characteristics from the ground scattering contribution. As expected, the angular separation for the bare field is almost zero resulting in a radial line passing through the origin; however, the secondary and primary forests also have insufficient separation (even near-zero for secondary). Given the HoA of 133 m for this test dataset, the PolInSAR-retrieved absolute phase-center height is around 7 m for the primary forest, which is too low to be even comparable to the previously-reported values (Treuhaft et al., 2015).

This is particularly pertinent to the unique extinction effect at X-band in the tropical forest, and also sheds light on the fact that the secondary forest in this area is denser (thus higher extinction) than the primary forest as previously reported in (Treuhaft et al., 2015; Treuhaft et al., 2017) so that its polarimetric phase separation is smaller due to the lack of ground scattering contribution. In other words, although the ground scattering exists for both primary and secondary forests, it is not strong enough to create a polarimetric dependence. This poor dual-pol PolInSAR performance has also been reported in the literature (Kugler et al., 2014; Chen et al., 2016).

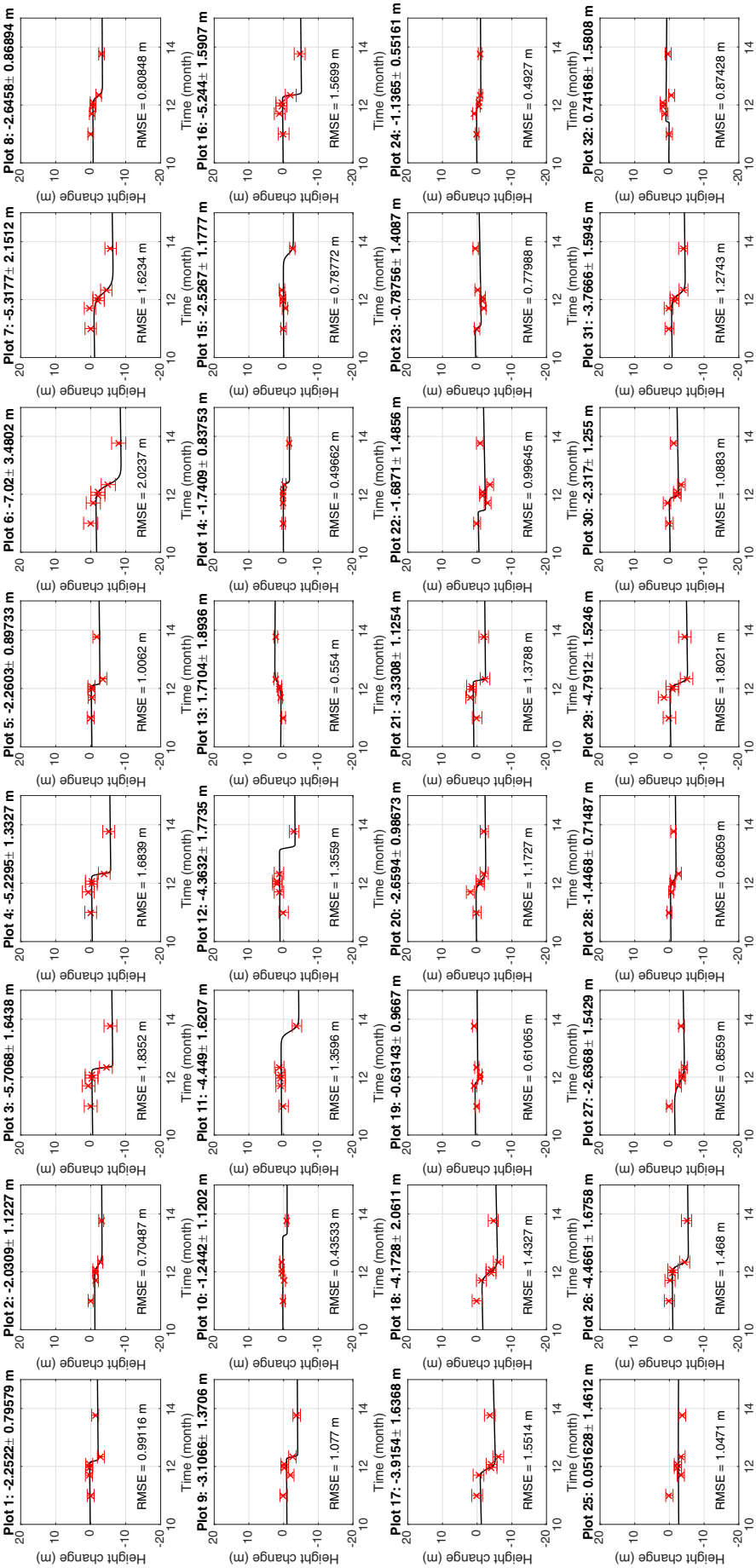

Fig. 10. The time-series plots for each of the 32 selective logging plots, where the amount of relative phase-center height drop along with its error is also marked. Horizontal axis denotes the month in 2015, e.g. "10" means October 2015, while "14" means February 2016. Both error bars and logistic fitting RMSE's are included. The error bars are generated due to the phase observational error given the measured InSAR coherence level.

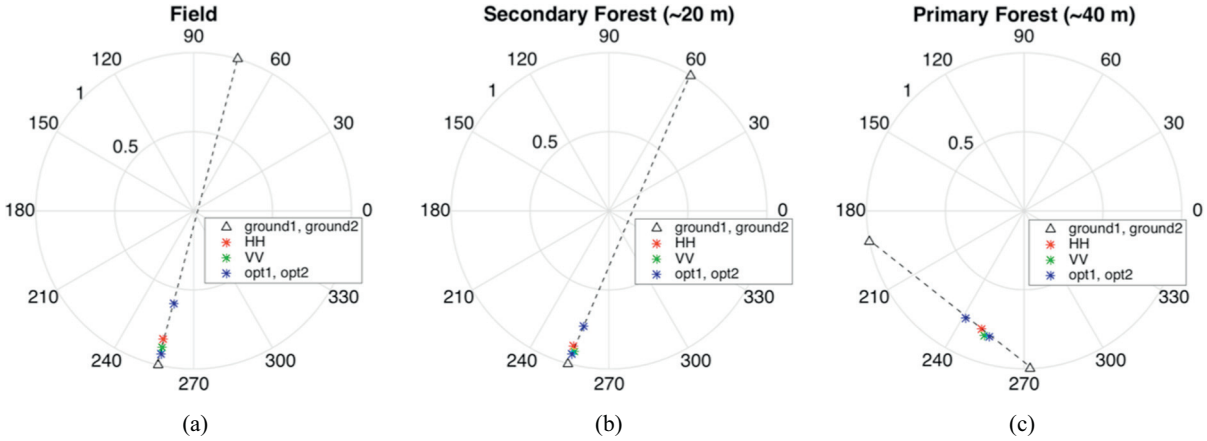

Fig. 11. PolInSAR complex-domain analysis for (a) bare field, (b) secondary forest (~20 m tall), and (c) primary forest (~40 m tall) in the Tapajos site using the TanDEM-X test dataset (20140915) with HoA of 133 m (Treuhaft et al., 2017). For each landscape, several markers are shown: the HH– and VV–pol complex InSAR coherences (denoted by "HH" and "VV"), the two Schur-optimized coherences of the elliptical coherence region (denoted by "opt1" and "opt2"), and the two candidate ground points (denoted by "ground1" and "ground2") on the unit circle. The coherences have been corrected for SNR decorrelation.

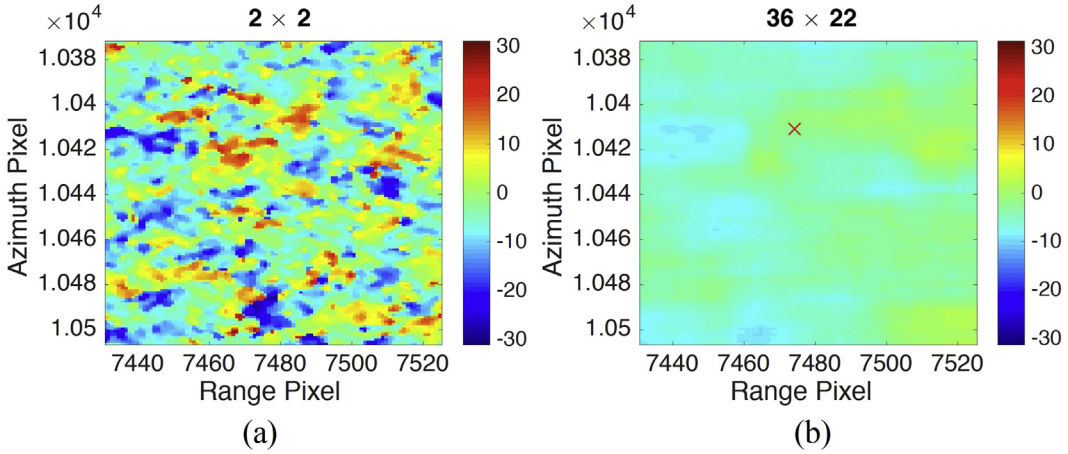

Fig. 12. The few-look interferogram (a) vs. the conventional look-averaged interferogram (b) over one of the 32 selective logging plots (marked as "red" cross in (b)). In (a), the 2 × 2 (4-) look averaging is used and followed by a 3 × 3 median filtering, while in (b), a 36 × 22 (quarter-hectare) look averaging is used. Both subplots are illustrated in the native (slant-range) radar coordinates with the phase flattened using SRTM DEM. The color scale is from −32 m to 32 m (for the entire range of HoA). (For interpretation of the references to color in this figure legend, the reader is referred to the web version of this article.)

4.2.3. Using a local constant from clear-cut stands

In contrast, because in this work all of the 32 plots are located in a relatively small area of the primary forest region (with mean top height of 20 m and maximum top height of 40 m; Gonçalves et al., 2017), a constant h_0 is thus assumed for this small area in this study so that the meter-level accuracy of determining the relative phase-center height change Δh will not be overwhelmed by the larger absolute height estimation error induced by any type of model-based inversion.

It has been shown that the TanDEM-X phase-center height is somewhere between the mean and maximum top height over this study area (Treuhaft et al., 2015). Also, as illustrated in Fig. 8 and focusing on a larger area around the selective logging site, the relative phase-center height between TanDEM-X (denoted by *TDX*) and SRTM (denoted by *SRTM*) has the minimum of −23 m ("dark blue"; due to clear cut between 2000 and 2015), i.e.,

$$TDX_{clear} - SRTM = -23\ \text{m} \tag{8}$$

and maximum of 5 m ("yellow to orange"; due to tree growth between 2000 and 2015), i.e.,

$$TDX_{grow} - SRTM = 5\ \text{m}. \tag{9}$$

Therefore, using SRTM height as a reference, if the clear-cut stands were not deforested, their absolute TanDEM-X phase-center height would have grown up to

$$h_0 = TDX_{grow} - TDX_{clear} = 5 - (-23) = 28\ \text{m}, \tag{10}$$

which is roughly the 75-percentile height at X-band (Praks et al., 2012). Please note that due to lack of auxiliary dataset and/or information and also because of the relatively small and homogeneous study area, this local-constant method is finally adopted to get the total phase height in this work. However, in order to fully automate the current DI retrieval approach, one has to resort to the other options discussed in this section.

4.2.4. Using few-look InSAR phase

Unlike using the conventional look-averaged InSAR phase, from previous studies (Treuhaft et al., 2009; Treuhaft et al., 2014), it has been suggested that few-look (e.g. 2 or 3) InSAR phase at C−/X−band with adequate bandwidth is capable of penetrating gaps (or "holes") among clustered "hard" targets with high extinction (e.g. dense tropical forest), and thus sensitive to the vegetation profile characteristics. This in turn enables seeing the ground in a few-look interferogram. The 4-look (2 × 2) TanDEM-X InSAR phase-inverted height is illustrated in Fig. 12 over one of the 32 logging stands, where the conventional look-averaged (36 × 22; 50 × 50 m resolution) InSAR phase-inverted height is also shown in comparison. In both subplots, the InSAR phase has

Table 3
Field measurements of selective logging: the columns are 1) *plot number*, 2) *time period of felling process (yymmdd)*, 3) *time period of skidding process (yymmdd)*, 4) *number of damaged trees (here, "damage" refers to crown loss due to felling and/or skidding)*, 5) *total number of trees*, 6) *DBH sum of the damaged trees (cm)*, 7) *DBH sum of all of the trees (cm)*, 8) *DBH-converted Disturbance Index (DI) metric.*

1	151101–151209	151212–151215	5	155	88.8	2924.2	0.03
2	N/A	N/A	0	133	0	2821.3	0
3	N/A	N/A	0	112	0	2512.4	0
4	151101–151209	151212–151215	8	116	203.4	2246.5	0.09
5	N/A	N/A	0	69	0	1735.5	0
6	151101–151209	151212–151215	7	100	356.7	2629.7	0.14
7	151101–151209	151212–151215	8	115	236.7	2598.8	0.09
8	N/A	N/A	0	135	0	2751.1	0
9	151112–160118	151223–160105	3	122	99.1	3247.1	0.03
10	151112–160118	151223–160105	13	116	396.6	2618.7	0.15
11	151112–160118	151223–160105	10	122	201.1	2497.6	0.08
12	151112–160118	151223–160105	2	102	35.8	2851.7	0.01
13	151112–160118	151223–160105	1	104	15.9	2503.7	0.01
14	151112–160118	151223–160105	10	148	178.8	3008.7	0.06
15	151112–160118	151223–160105	2	138	30.1	3019.4	0.01
16	151112–160118	151223–160105	11	100	445.7	2377	0.19
17	151118–151209	151209–151211	25	138	757.1	3164.9	0.24
18	151118–151209	151209–151211	16	133	286.7	3010	0.1
19	151118–151209	151209–151211	1	90	54	2065.6	0.03
20	151118–151209	151209–151211	15	119	307.7	2668.9	0.12
21	151109–151119	151124–151127	6	123	254.6	3045.6	0.08
22	151109–151119	151124–151127	6	95	161.1	2265.3	0.07
23	151109–151119	151124–151127	1	116	24.6	2840.5	0.01
24	151109–151119	151124–151127	6	101	159.1	2961	0.05
25	N/A	N/A	0	92	0	2202.1	0
26	151109–151119	151124–151127	17	129	334.2	2582.7	0.13
27	N/A	N/A	0	144	0	3190.2	0
28	N/A	N/A	0	99	0	2609.5	0
29	151118–151209	151209–151211	25	138	552.1	2934.7	0.19
30	151118–151209	151209–151211	11	106	314.2	2714.4	0.12
31	151118–151209	151209–151211	7	121	134.4	2844.4	0.05
32	N/A	N/A	0	132	0	3137.4	0

been flattened using the SRTM DEM to remove the topographic phase so that there is no significant phase wrapping problem as it can be seen that the phase-inverted height varies gradually and continuously in space for most of the time. In order to reduce the high-frequency speckle noise in the few-look interferogram, a 3 × 3 median filter was applied, which indicates the resulting large dynamic range of the few-look InSAR phase (manifested by the clusters that spatially span over tens of looks or equivalently tens of meters) captures the real distribution (rather than noise) of InSAR phase-center height.

Here, the ground phase estimate is manually selected from the few-look interferogram over the small selective logging area, while the development of the automated processing routine is in progress and thus serves an important future work. From Fig. 12a, it can be seen that the local minima are around −26 m, while the conventional look-averaged phase-center is around 0 m over the logging stand. So the absolute phase-center height can be estimated as $h_0 = 0 - (-26) = 26$ m. Note the few-look phase uncertainty is expected to be larger than the conventional look-averaged one, both of which are constrained by the coherence value and the number of looks used in the averaging. Based on the Cramer-Rao bound (Rosen et al., 2000), and given a mean coherence value of 0.6 over the logging area, the error of the determined phase-center height is around 4.5 m in the 4-look interferogram. However, a histogram method can be used to average all of the local minima, which has the potential to further reduce the uncertainty in future work.

Here we have demonstrated a new way (although a bit heuristic at this stage, more rigorous treatment has been under development) to extract the ground InSAR phase from TanDEM-X data. Using this technique to get the ground-level phase while also assuming the ground scattering contribution is negligible, the Random Volume model (Treuhaft et al., 1996) can be inverted for the test dataset in Fig. 11 to retrieve both forest height and extinction coefficient, which is around 0.05 dB/m for the primary forest in our study area, and 0.1 dB/m for the secondary forest (thus "denser" than primary forests) with few-meter height estimation RMSE over quarter-hectare forest stands. This is consistent with the above PolInSAR complex-domain analysis as well as the previous work over the same area (Treuhaft et al., 2015). As for these low extinction values, previous studies have pointed out that given adequate bandwidth, C−/X−band signals can penetrate gaps (or "holes") among clustered "hard" targets with high extinction (e.g. dense tropical forest), which could effectively result in a low-extinction random volume (Treuhaft et al., 2009; De Zan et al., 2013; Treuhaft et al., 2014).

4.2.5. Using SAR tomography

In principle, TanDEM-X (or essentially the future TanDEM-L with more penetration) data archive can be considered as a stack of multi-baseline dataset for applying SAR tomography techniques (Pardini et al., 2013a; Pardini et al., 2013b) assuming the temporal changes are negligible during multiple repeats. Therefore, the underlying ground topography can be retrieved from the three-dimensional tomogram generated using a Capon estimator (Pardini et al., 2013b). In fact, the historical TanDEM-X dataset have a large baseline-diversity over the current study area at Tapajos, although the data stack used in this paper are the only six baselines available at the time of the selective logging events. Due to the limit on the length and scope of the paper, this method was not further validated here, and is an important future work by itself.

4.3. Validation of forest disturbance results with field inventory data

Therefore, given the phase-center height change for each plot in Fig. 10 and the constant $h_0 = 28$ m (a region estimate from the clear-cut method; with the same accuracy as TanDEM-X DEM that is around 1–2 m) as the absolute phase-center height, the TanDEM-X-measured DI metric can thus be calculated by using Eq. (7) and further compared with those determined from field record by using Eq. (4). The plot-level disturbance record is summarized below in Table 3.

The comparison between TanDEM-X results and field inventory record is illustrated in Fig. 13, where the error bars of the TanDEM-X results are included by running Monte Carlo simulations based on the observational error bars in Fig. 10. In particular, for each of the 32 plots, 1000 Monte Carlo simulations are performed to generate the InSAR data points that obey the same error bars (or distributions) in Fig. 10. Then, a standard non-linear least squares fit was carried out to fit the generalized logistic function to each set of InSAR data points with the fitting parameters determined. Therefore, 1000 realizations of the fitting parameters can be obtained for each plot. Noticing the error in DI (or equivalently Δh by ignoring the error in h_0) relates to the error in parameter C while the error in disturbance epoch relates to the error in parameter E of Eq. (6), we can thus generate the error bars as shown in Fig. 13.

It can be seen that the DI estimates were determined with a Normalized RMSE (NRMSE) of 30% over 32 quarter-hectare stands (with the probability of 0.2% in realizing the same or better R measure and RMSE by accident), which suggests statistical significance of the comparison and thus the applicability of the simple model in Eq. (7) for this particular study area with small dynamic range of DI (0–0.25).

Regarding the error analysis, the error bars are generated by Monte Carlo simulations of the InSAR phase height change Δh, which accounts for a large portion of the realistic error sources. This is because these error bars are just about to clip the "1:1" line resulting in a reduced chi-squared of 2.39. In order to obtain a reduced chi-squared of 1.0 for a statistically good curve fitting, the error bars need to be further stretched by a factor of $\sqrt{2.39} \approx 1.55$, which implies that there is still some residual (both statistical and modeling) error that has not been accounted for although the phase height change accounts for the majority

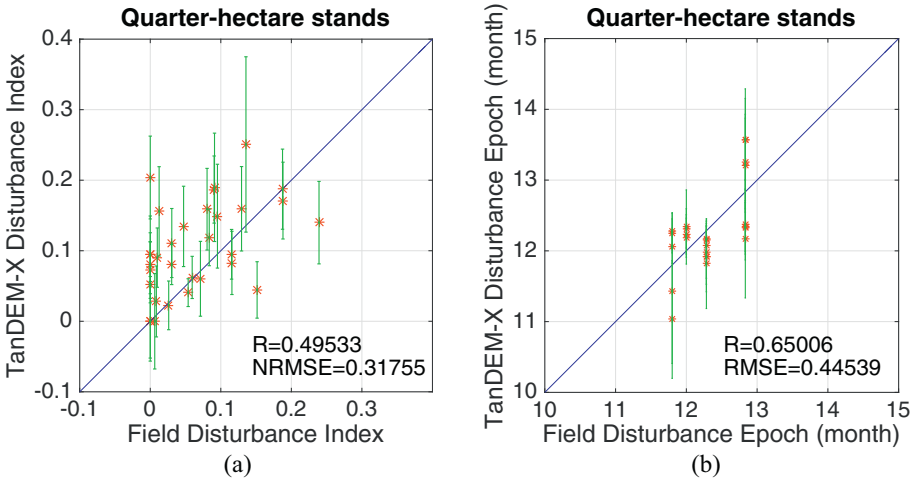

Fig. 13. Scatterplots of TanDEM-X measured disturbance indices compared against the field-determined indices (a), as well as the TanDEM-X measured disturbance epochs against with the field-recorded epochs (b). Both subplots have the error bars included along with the error metrics, i.e., RMSE and R (Pearson correlation coefficient), calculated over the 32 quarter-hectare plots.

(1/1.55 ≈ 65%) of the total error. The error in estimating h_0 and κ_z do not play a big role in this study for the specific reasons mentioned earlier, while the measurement error in the field data could be an essential source that degrades the field-derived DI. Besides the statistical measurement error, there could also be some modeling error from the assumptions in the DI definition with the "top-down" concept, as well as the ground contribution-dependent $\frac{\Delta h}{h_0}$ - *DI* relationship in Fig. 7. All of the above error sources can be carefully revisited in the future work for a better performance of the approach. However, given the current RMSE level, the statistical significance and R measure are expected to considerably improve if a larger dynamic range of DI is tested as the current range (0–0.25) is quite short, which suggests the future validation of this approach for various levels of logging over a large variety of forest types.

The disturbance epoch is estimated with a RMSE of 0.44 month (13.2 days), which is in fact constrained by the temporal resolution (or repeat interval) of TanDEM-X mission (around 2 weeks for most of the time). Here, the field-measured disturbance epoch is the average of the starting date and the ending date (Table 3) postponed by 10 days. Because the recorded starting and ending dates only roughly capture the entire time period (that spans over months), if the average of them was used, an RMSE of 16 days can be achieved. In this work, the average of the starting and ending dates postponed by 10 days is found to produce the "best fit" (in terms of both RMSE and the R measure) compared to the TanDEM-X measured disturbance epochs (i.e., the *E* parameter of the logistic fit in Eq. (6)).

4.4. Comparison of TanDEM-X results with ALOS-2 data

Although a single-pass InSAR mission at L-band (such as the future TanDEM-L) would be more pertinent to validate and improve this approach for quantitative DI retrieval, in this section, we show the repeat-pass L-band results from ALOS-2 which are the concurrent InSAR measurements available. Hence, the objective here is not to further improve the quantitative results but to qualitatively validate the single-pass InSAR results as both radar sensors are expected to confirm the area and epoch of the selective logging events. Through the comparison, one can also see that the single-pass InSAR results are much more quantitative and robust than the repeat-pass ones for this type of application and at this challenging study area in tropics.

As for the ALOS-2 InSAR coherence maps, because the interferometric vertical wavenumbers are very small (i.e., $\kappa_z < 0.01$ rad/m; see Table 2), the geometric decorrelation can be ignored. Therefore, the observed InSAR correlations after reasonable co-registration were then corrected for correlation magnitude bias (Touzi et al., 1999; Lei, 2016) and thermal noise decorrelation (Zebker and Villasenor, 1992; Lei, 2016), resulting in the coupled InSAR correlation component primarily attributable to temporal changes due to moisture- and wind-induced effects as well as forest disturbance (as volume scattering can be ignored for such small κ_z's). The four HH-pol ALOS-2 InSAR pairs that have relatively higher coherence values are illustrated in Fig. 14 with their scene-wide mean coherence values tabularized in Table 2, and the coherence is much lower than 0.1 for other possible InSAR pairs (thus not used in this work).

As seen in Table 2, the scene-wide InSAR correlation magnitude is calculated as low as 0.1–0.3, which is due to several factors. First, normal temporal decorrelation (i.e., moisture-induced dielectric change and wind-induced random motion) accounts for the low scene-wide background coherence, which is further related to the local weather and/or climate in this tropical area. Despite the generally dry conditions throughout the acquisition period, the local temporal variation of moisture and/or wind as a combination could result in a non-trivial fluctuating dynamics that quickly decorrelates the repeat-pass radar acquisitions in this region. Second, as shown in Fig. 9 and also below, extensive forest fire accounts for those extremely low-coherence regions. During the selective logging period, because the weather was very dry, the rainy season was delayed after December 2015, and thus there were a large amount of forest fires over Tapajos National Forest as confirmed with the concurrent MODIS data (Giglio et al., 2016). Besides the above two major causes, there may also be some other error sources, such as equatorial ionospheric scintillation that achieves cyclical maximum during the timeframe of 2014–2016 (Meyer et al., 2016), residual mis-registration between the repeat-pass SAR images, other natural and/or human-induced disturbance activities, etc.

However, we will show how the current dataset could be utilized to reveal forest disturbance signatures and further compared with the TanDEM-X results. In particular, the forest mean temporal correlation (as shown in Table 2) was determined by averaging over the entire InSAR scene (tens of kilometers wide) and also masking out the non-forest areas. This is achieved by using the SAR backscatter imagery combined with the InSAR coherence map (through thresholding) as a forest/non-forest mask, which also excludes the extremely low-coherence regions due to fire. Therefore, the residual InSAR coherence component after compensating (dividing by) the forest mean temporal correlation can be considered as an indicator of extra temporal decorrelation factors such as selective logging and fire (Lei et al., 2018). The results are shown in Fig. 15, where the fire locations as observed by MODIS are also marked as "red" dots outside the selective logging area for each InSAR pair. It can be seen that most of the MODIS fire locations correspond well with the extremely low-coherence regions of the ALOS-2 images. Because the ALOS-2 InSAR coherence is very low, the observational error will prohibit quantitative and accurate classification. As expected, there are a number of "false" detections over the selective

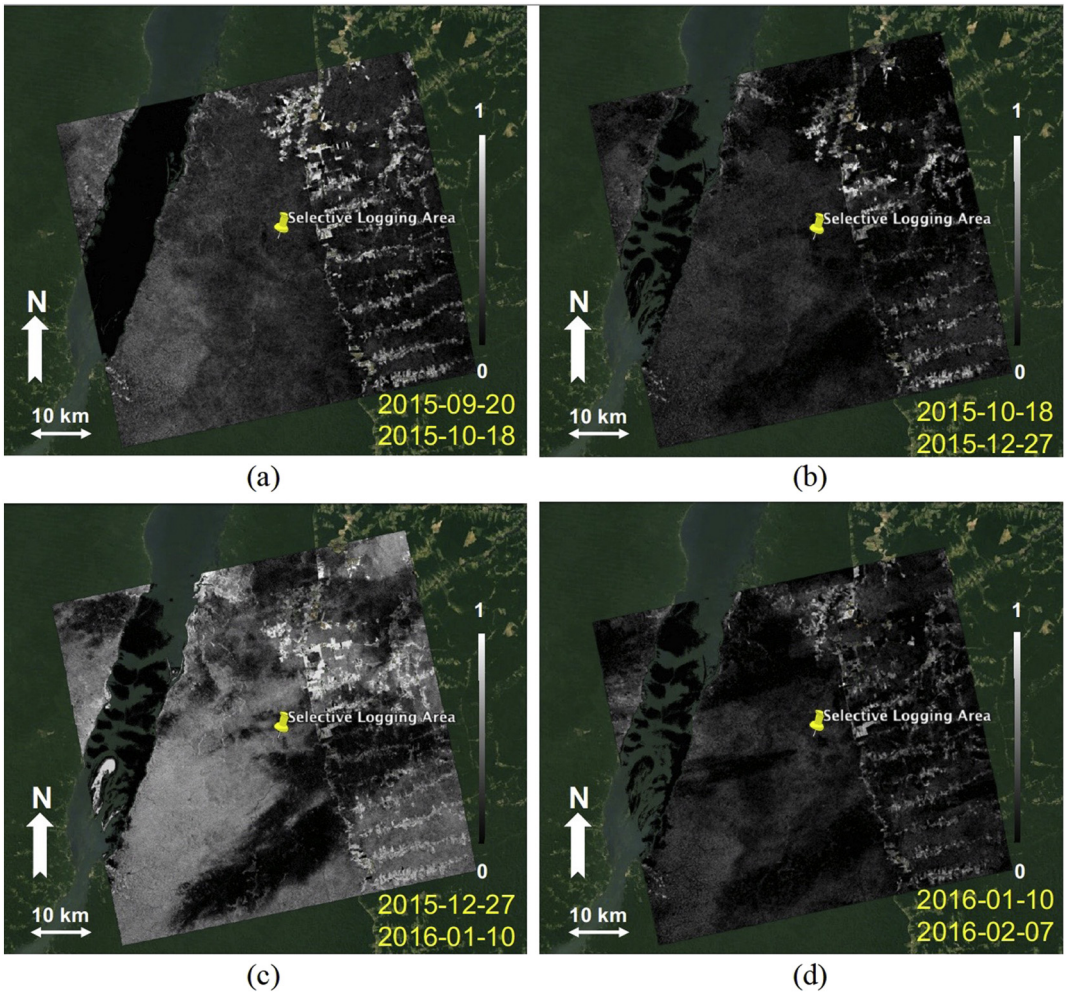

Fig. 14. HH-pol ALOS-2 InSAR correlation magnitude (after calibration) over the Tapajos test site. The grey scale (0 to 1) is indicated, so are the pair of acquisition dates.

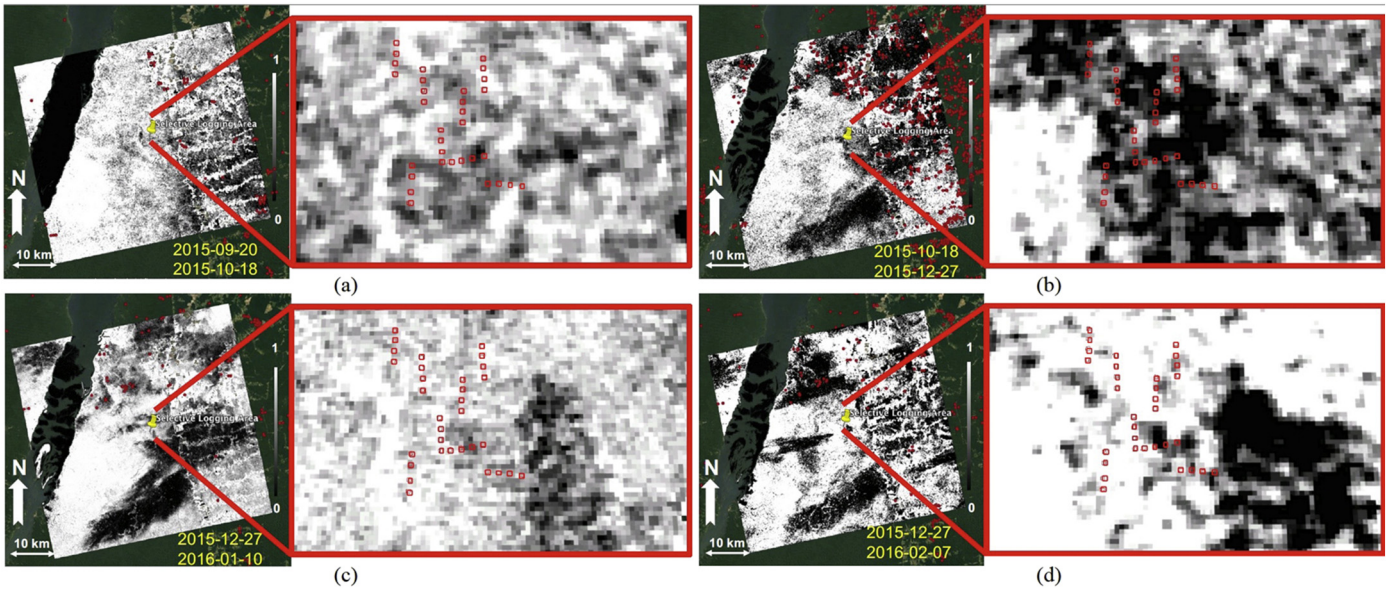

Fig. 15. ALOS-2 InSAR correlation component due to disturbance, where the forest mean (normal) temporal correlation has been compensated (i.e., used to divide the coherence in Fig. 14). The grey scale is from 0 to 1 as indicated. The closeup subfigures are shown over the 32 selective logging plots ("red" squares). The "red" dots outside the selective logging area represent concurrent fire locations identified by MODIS. (For interpretation of the references to color in this figure legend, the reader is referred to the web version of this article.)

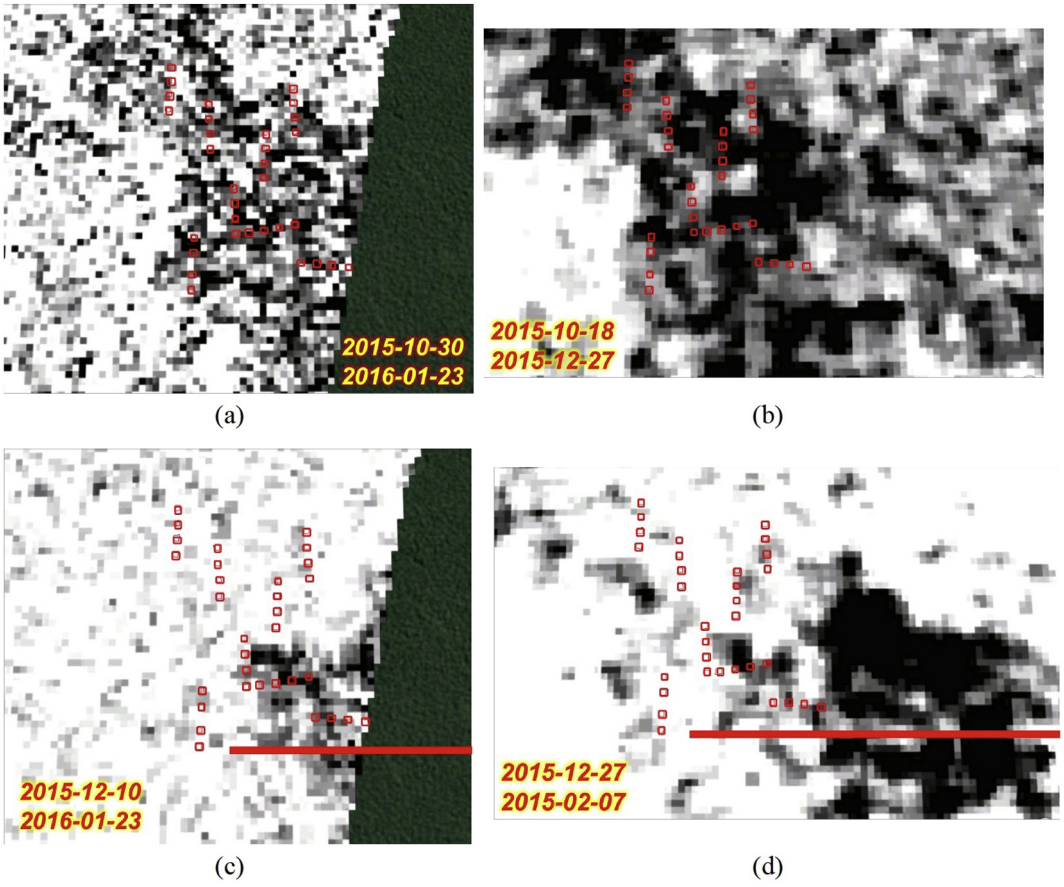

Fig. 16. Qualitative comparison between TanDEM-X differential phase-center height (a and c; color scale from −5 m to 0 m) and ALOS-2 InSAR correlation component due to disturbance (b and d; color scale from 0 to 1). (a) and (b) correspond to the entire selective logging period, while (c) and (d) capture the end of the logging period along with some post-logging activities. The time period for each image is shown. In particular, (a) is the difference between Fig. 8f and Fig. 8a, (b) is from Fig. 15b, (c) is from Fig. 9d, and (d) is from Fig. 15d. The access road to the logging area via the ICMBio base (shown in Fig. 1) is indicated by the "red" line. (For interpretation of the references to color in this figure legend, the reader is referred to the web version of this article.)

logging area due to the large measurement uncertainty.

However, by comparing the blowup subplots in Fig. 15 with those in Fig. 9 and matching up the time period, it can be seen that both TanDEM-X and ALOS-2 (although qualitatively) detect the selective logging event over the same area and time period (that is late October 2015 through late January 2016) as well as the fact that selective logging activities moving from northwest to southeast as further confirmed by the field work. A closer look at the two sensors' results is illustrated in Fig. 16.

In particular, Fig. 16a is the entire disturbance-affected area from TanDEM-X phase-center height change (i.e., differential height between Fig. 8a and Fig. 8f), and Fig. 16b is the entire disturbance-affected area from ALOS-2 coherence (same as Fig. 15b). It is clear that both sensors capture the area of forest disturbance during the logging period. Further, Fig. 16c (same as Fig. 9d) and Fig. 16d (same as Fig. 15d) illustrate disturbance to the end of the logging period along with some post-logging activities, such as the skidding process (see Table 3 for the dates) and transporting the logs to the ICMBio base along the access road ("red" lines in both Fig. 1 and Fig. 16). This is clear from the ALOS-2 image, Fig. 16d, which not only captures the forest disturbance (that is captured by the TanDEM-X image as in Fig. 16c) but also the human activity-induced post-logging activities (to the east of the logging sites).

5. Discussions and conclusions

This paper demonstrates an approach to quantify selective logging using spaceborne single-pass SAR interferometry. A physically-defined metric was introduced to quantify the amount of forest disturbance (such as logging and fire), namely disturbance index or DI. Using spaceborne single-pass SAR interferometry, the relative change of HH-pol InSAR phase-center height from DLR's TanDEM-X times-series data are exploited to generate disturbance indices with Normalized RMSE of 30% for DI $\leq$ 0.3 as validated against field measurements over 32 quarter-hectare selective logging stands at Tapajos, Brazil. As a comparison dataset, JAXA's concurrent ALOS-2 HH-pol InSAR correlation magnitude (after compensation for the other unrelated decorrelation effects) were also shown to detect forest disturbance. However, due to the extremely low coherence in this tropical area, the ALOS-2 results only qualitatively depict the area and epoch of the selective logging process (with several false detections; thus only considered as an *auxiliary dataset*), while the TanDEM-X results are found to be much more stable and accurate for mapping the tropical forest disturbance (considered as a *primary dataset*).

Future improvements of the results presented in the current study are enumerated as below. First, the single-pass InSAR approach needs to be tested over a larger dynamic range of the disturbance index and over various forest types so that the actual functional relationship between the field-measured disturbance index and the relative InSAR phase height drop can be better understood. This also brought up the significance of having a meticulously-planned field work (such as the "permanent plot" method; Sheil, 1995) through which the field data-based InSAR simulation (as presented in this work) can thus be performed to study this relationship from a modeled perspective. Second, the ground phase estimation based on the few-look interferogram needs to be carefully revisited and then automated thus requiring a more robust method to extract those ground-level phases (that can be seen

through canopy gaps), which will further aid in forest height inversion using TanDEM-X InSAR data and/or in fusion with NASA's future lidar mission, GEDI (Qi and Dubayah, 2016). Other options for extracting the ground phase are also strongly recommended for automation, such as using the lidar DTM, global ground phase determination from P-band InSAR (e.g. ESA's future BIOMASS mission; Minh et al., 2015) and SAR tomography. Third, in relation to the error analysis in Section 4.3, both the statistical measurement error (e.g. Δh, h_0, κ_z and field-measured forest characteristics) and modeling error (e.g. assumptions in the DI definition with the "top-down" logging concept, and the modeled $\frac{\Delta h}{h_0}$ - *DI* relationship) in this study need to be carefully revisited and compensated to further ensure a statistically good performance of the approach. Last, it may be possible to quantitatively cross-validate the repeat-pass InSAR approach (Lei et al., 2018) with the single-pass InSAR approach over some areas with stable weather/climate.

The method described in this paper is simple and efficient (thus has been mostly automated), which only requires single-baseline, single-polarization InSAR data (thus more frequent acquisitions can be obtained). Please note, as for automated processing, there are still steps that cannot be easily automated at this moment, such as the total phase height estimation or ground phase determination, which is currently under development at the time of writing this draft. Also, it should be noted that in this study, prior knowledge of where and when selective logging happened instead of forest fire or other causes was used to distinguish selective logging from other disturbance events. In practice, without the prior information, using this approach itself is not sufficient to tell which phase height drop is due to selective logging and which is not. Therefore, rather than generating a product of "selective logging index" by discriminating the false detections (e.g. based on their lateral distribution or using multiple sensor data, which is very difficult if not impossible), in this work, we defined a generic term of disturbance index or DI, and examined the potential for automated generation of DI products wherever there is an InSAR phase height drop due to various (either natural or man-made) causes, e.g. the same approach is also able to detect the severity of forest fire as shown earlier. In terms of carbon cycle dynamics and climate change, all of these causes will have essential contributions and thus are meant to be included in the final DI products (through using the current approach on the robust InSAR time-series of phase height change), while the interpretation of these products would require some human and/or artificial intelligence, such as expertise in forest ecology.

More importantly, this method has been shown to detect and quantify forest disturbance (not necessarily selective logging) at a large scale (tens of kilometers) with fine spatial resolution (< 1 ha), and thus has the potential to provide a global coverage. This approach could also serve as an observing prototype on forest disturbance study for current and future spaceborne single-pass InSAR missions (e.g. DLR's TanDEM-X and in the future, TanDEM-L), as well as provide a practical solution to monitor large-scale (potentially continental-scale) forest disturbance as relevant to UN's REDD+ programme.

Acknowledgement

The authors would like to thank Piyush Agram from the ISCE developer team at Jet Propulsion Laboratory for the valuable discussions and generous support on InSAR processing of TanDEM-X and ALOS-2 data using the ISCE software package. Gratitude also goes to the TanDEM-X staff (particularly Thomas Busche and Thomas Fritz) at the German Aerospace Center (DLR) for processing and delivery of the TanDEM-X data and for technical discussions. The authors also thank DLR and Japanese Aerospace Exploration Agency (JAXA) for the coordination in acquiring the TanDEM-X and ALOS-2 data over the Tapajos test site around the scheduled selective logging period. We would also like to thank the anonymous reviewers for the valuable and professional suggestions. This work is supported by an appointment to the NASA Postdoctoral Program at the Jet Propulsion Laboratory, California Institute of Technology, administered by Universities Space Research Association under contract with NASA.

References

Andersen, H.E., Reutebuch, S.E., McGaughey, R.J., d'Oliveira, M.V., Keller, M., 2014. Monitoring selective logging in western Amazonia with repeat lidar flights. Remote Sens. Environ. 151, 157–165.
Askne, J.I., Fransson, J.E., Santoro, M., Soja, M.J., Ulander, L.M., 2013. Model-based biomass estimation of a hemi-boreal forest from multitemporal TanDEM-X acquisitions. Remote Sens. 5 (11), 5574–5597.
Askne, J.I., Soja, M.J., Ulander, L.M., 2017. Biomass estimation in a boreal forest from TanDEM-X data, lidar DTM, and the interferometric water cloud model. Remote Sens. Environ. 196, 265–278.
Asner, G.P., Keller, M., Pereira, R., Zweede, J.C., 2002. Remote sensing of selective logging in Amazonia: assessing limitations based on detailed field observations, Landsat ETM+, and textural analysis. Remote Sens. Environ. 80 (3), 483–496.
Asner, G.P., Knapp, D.E., Broadbent, E.N., Oliveira, P.J., Keller, M., Silva, J.N., 2005. Selective logging in the Brazilian Amazon. Science 310 (5747), 480–482.
Asner, G.P., Keller, M., Lentini, M., Merry, F., Souza, C., 2009. Selective logging and its relation to deforestation. In: Amazonia and global change, pp. 25–42.
Chen, H., Cloude, S.R., Goodenough, D.G., 2016. Forest canopy height estimation using Tandem-X coherence data. IEEE J. Selec. Topics Appl. Earth Observ. Rem. Sens. 9 (7), 3177–3188.
Cloude, S., 2010. Polarisation: Applications in Remote Sensing. Oxford University Press.
Cloude, S.R., Chen, H., Goodenough, D.G., 2013. Forest height estimation and validation using Tandem-X polinsar. In: IEEE Geoscience and Remote Sensing Symposium (IGARSS), 2013 IEEE International, pp. 1889–1892.
De Zan, F., Krieger, G., López-Dekker, P., 2013. On some spectral properties of TanDEM-X interferograms over forested areas. IEEE Geosci. Remote Sens. Lett. 10 (1), 71–75.
Farr, T.G., Rosen, P.A., Caro, E., Crippen, R., Duren, R., Hensley, S., Kobrick, M., Paller, M., Rodriguez, E., Roth, L., Seal, D., 2007. The shuttle radar topography mission. Rev. Geophys. 45 (2).
Fatoyinbo, T.E., Simard, M., 2013. Height and biomass of mangroves in Africa from ICESat/GLAS and SRTM. Int. J. Remote Sens. 34 (2), 668–681.
Giglio, L., Schroeder, W., Justice, C.O., 2016. The collection 6 MODIS active fire detection algorithm and fire products. Remote Sens. Environ. 178, 31–41.
Gonçalves, F.G., 2014. Vertical Structure and Aboveground Biomass of Tropical Forests from Lidar Remote Sensing (Doctoral Dissertation).
Gonçalves, F., Treuhaft, R., Law, B., Almeida, A., Walker, W., Baccini, A., dos Santos, J.R., Graça, P., 2017. Estimating aboveground biomass in tropical forests: field methods and error analysis for the calibration of remote sensing observations. Remote Sens. 9 (1), 47.
Holmes, T.P., Blate, G.M., Zweede, J.C., Pereira, R., Barreto, P., Boltz, F., Bauch, R., 2002. Financial and ecological indicators of reduced impact logging performance in the eastern Amazon. For. Ecol. Manag. 163 (1), 93–110.
Hooper, A., Zebker, H., Segall, P., Kampes, B., 2004. A new method for measuring deformation on volcanoes and other natural terrains using InSAR persistent scatterers. Geophys. Res. Lett. 31 (23).
Houghton, R.A., Greenglass, N., Baccini, A., Cattaneo, A., Goetz, S., Kellndorfer, J., Laporte, N., Walker, W., 2010. The role of science in reducing emissions from deforestation and forest degradation (REDD). Cardiol. Manag. 1 (2), 253–259.
Keller, M., Palace, M., Hurtt, G., 2001. Biomass estimation in the Tapajos National Forest, Brazil: examination of sampling and allometric uncertainties. For. Ecol. Manag. 154 (3), 371–382.
Keller, M., Asner, G.P., Silva, N., Palace, M., 2004. Sustainability of selective logging of upland forest in the Brazilian Amazon. In: Working forests in the Neotropics: Conservation through sustainable management, pp. 41–63.
Krieger, G., Moreira, A., Fiedler, H., Hajnsek, I., Werner, M., Younis, M., Zink, M., 2007. TanDEM-X: a satellite formation for high-resolution SAR interferometry. IEEE Trans. Geosci. Remote Sens. 45 (11), 3317–3341.
Krieger, G., De Zan, F., Bachmann, M., Dekker, P.L., Cassola, M.R., Kim, J.S., 2014. Tropospheric and ionospheric effects in spaceborne single-pass SAR interferometry and radargrammetry. In: EUSAR 2014; 10th European Conference on Synthetic Aperture Radar; Proceedings of (pp. 1–4). VDE.
Kugler, F., Schulze, D., Hajnsek, I., Pretzsch, H., Papathanassiou, K.P., 2014. TanDEM-X pol-InSAR performance for forest height estimation. IEEE Trans. Geosci. Remote Sens. 52 (10), 6404–6422.
Lee, S.K., Fatoyinbo, T.E., 2015. TanDEM-X Pol-InSAR inversion for mangrove canopy height estimation. IEEE J. Selec. Topics Appl. Earth Observ. Rem. Sens. 8 (7), 3608–3618.
Lei, Y., 2016. Electromagnetic scattering models for InSAR correlation measurements of vegetation and snow. In: Ph.D. Dissertation. University of Massachusetts Amherst.
Lei, Y., Lucas, R., Siqueira, P., Schmidt, M., Treuhaft, R., 2018. Detection of forest disturbance with spaceborne repeat-pass SAR interferometry. IEEE Trans. Geosci. Remote Sens. 56 (4), 2424–2439.
Meyer, F.J., Chotoo, K., Chotoo, S.D., Huxtable, B.D., Carrano, C.S., 2016. The influence of equatorial scintillation on L-band SAR image quality and phase. IEEE Trans. Geosci. Remote Sens. 54 (2), 869–880.
Minh, D.H.T., Tebaldini, S., Rocca, F., Le Toan, T., Villard, L., Dubois-Fernandez, P.C., 2015. Capabilities of BIOMASS tomography for investigating tropical forests. IEEE Trans. Geosci. Remote Sens. 53 (2), 965–975.
Pan, Y., Birdsey, R.A., Fang, J., Houghton, R., Kauppi, P.E., Kurz, W.A., Phillips, O.L.,

Shvidenko, A., Lewis, S.L., Canadell, J.G., Ciais, P., 2011. A large and persistent carbon sink in the world's forests. Science 333 (6045), 988–993.
Papathanassiou, K.P., Cloude, S.R., 2001. Single-baseline polarimetric SAR interferometry. IEEE Trans. Geosci. Remote Sens. 39 (11), 2352–2363.
Pardini, M., Kugler, F., Papathanassiou, K., 2013a. Towards forest vertical structure monitoring from space: first experiments with multi-baseline TanDEM-X data. POLinSAR 2013 (49), 53.
Pardini, M., Torano-Caicoya, A., Kugler, F., Papathanassiou, K., 2013b. Estimating and understanding vertical structure of forests from multibaseline TanDEM-X Pol-InSAR data. In: Geoscience and Remote Sensing Symposium (IGARSS), 2013 IEEE International, pp. 4344–4347.
Pereira, R., Zweede, J., Asner, G.P., Keller, M., 2002. Forest canopy damage and recovery in reduced-impact and conventional selective logging in eastern Para, Brazil. For. Ecol. Manag. 168 (1), 77–89.
Potapov, P., Yaroshenko, A., Turubanova, S., Dubinin, M., Laestadius, L., Thies, C., Aksenov, D., Egorov, A., Yesipova, Y., Glushkov, I., Karpachevskiy, M., 2008. Mapping the world's intact forest landscapes by remote sensing. Ecol. Soc. 13 (2), 51.
Praks, J., Hallikainen, M., Kugler, F., Papathanassiou, K.P., 2007. X-band extinction in boreal forest: estimation by using E-SAR POLInSAR and HUTSCAT. In: Geoscience and Remote Sensing Symposium (IGARSS), 2007 IEEE International, pp. 1128–1131.
Praks, J., Antropov, O., Hallikainen, M.T., 2012. LIDAR-aided SAR interferometry studies in boreal forest: scattering phase center and extinction coefficient at X-and L-band. IEEE Trans. Geosci. Remote Sens. 50 (10), 3831–3843.
Qi, W., Dubayah, R.O., 2016. Combining Tandem-X InSAR and simulated GEDI lidar observations for forest structure mapping. Remote Sens. Environ. 187, 253–266.
Rosen, P.A., Hensley, S., Joughin, I.R., Li, F.K., Madsen, S.N., Rodriguez, E., Goldstein, R.M., 2000. Synthetic aperture radar interferometry. Proc. IEEE 88 (3), 333–382.
Rosen, P.A., Shams, K.S., Gurrola, E.M., George, B.A., Knight, D.S., 2012. InSAR scientific computing environment on the cloud. In: AGU Fall Meeting Abstracts. Vol. 1. pp. 1508.
Rutishauser, E., Hérault, B., Baraloto, C., Blanc, L., Descroix, L., Sotta, E.D., Ferreira, J., Kanashiro, M., Mazzei, L., d'Oliveira, M.V., De Oliveira, L.C., 2015. Rapid tree carbon stock recovery in managed Amazonian forests. Curr. Biol. 25 (18), R787–R788.
Sadeghi, Y., St-Onge, B., Leblon, B., Simard, M., Papathanassiou, K., 2014. Mapping forest canopy height using TanDEM-X DSM and airborne LiDAR DTM. In: In 2014 IEEE Geoscience and Remote Sensing Symposium, pp. 76–79.
Schimel, D., Stephens, B.B., Fisher, J.B., 2015. Effect of increasing CO2 on the terrestrial carbon cycle. Proc. Natl. Acad. Sci. 112 (2), 436–441.
Schmidt, M., Lucas, R., Bunting, P., Verbesselt, J., Armston, J., 2015. Multi-resolution time series imagery for forest disturbance and regrowth monitoring in Queensland, Australia. Remote Sens. Environ. 158, 156–168.
Sheil, D., 1995. A critique of permanent plot methods and analysis with examples from Budongo Forest, Uganda. For. Ecol. Manag. 77 (1), 11–34.
Silva, C.A., Hudak, A.T., Vierling, L.A., Klauberg, C., Garcia, M., Ferraz, A., Keller, M., Eitel, J., Saatchi, S., 2017. Impacts of airborne lidar pulse density on estimating biomass stocks and changes in a selectively logged tropical forest. Remote Sens. 9 (10), 1068.
Silver, W.L., Neff, J., McGroddy, M., Veldkamp, E., Keller, M., Cosme, R., 2000. Effects of soil texture on belowground carbon and nutrient storage in a lowland Amazonian forest ecosystem. Ecosystems 3 (2), 193–209.
Solberg, S., Weydahl, D.J., Nasset, E., 2010. Simulating X-band interferometric height in a spruce forest from airborne laser scanning. IEEE Trans. Geosci. Remote Sens. 48 (9), 3369–3378.
Solberg, S., Astrup, R., Breidenbach, J., Nilsen, B., Weydahl, D., 2013a. Monitoring spruce volume and biomass with InSAR data from TanDEM-X. Remote Sens. Environ. 139, 60–67.
Solberg, S., Astrup, R., Weydahl, D.J., 2013b. Detection of forest clear-cuts with shuttle radar topography mission (SRTM) and Tandem-X InSAR data. Remote Sens. 5 (11), 5449–5462.
Solberg, S., Næsset, E., Gobakken, T., Bollandsås, O.M., 2014. Forest biomass change estimated from height change in interferometric SAR height models. Carbon Balance Manag. 9 (1), 5.
Souza Jr, C., Barreto, P., 2000. An alternative approach for detecting and monitoring selectively logged forests in the Amazon. Int. J. Remote Sens. 21 (1), 173–179.
Souza, C., Firestone, L., Silva, L.M., Roberts, D., 2003. Mapping forest degradation in the eastern Amazon from SPOT 4 through spectral mixture models. Remote Sens. Environ. 87 (4), 494–506.
SRTM, 2014. https://e4ftl01.cr.usgs.gov/SRTM/ [last accessed on December 3rd 2016].
Stone, T.A., Lefebvre, P., 1998. Using multi-temporal satellite data to evaluate selective logging in Para, Brazil. Int. J. Remote Sens. 19 (13), 2517–2526.
Touzi, R., Lopes, A., Bruniquel, J., Vachon, P.W., 1999. Coherence estimation for SAR imagery. IEEE Trans. Geosci. Rem. Sens. 37 (1), 135–149.
Treuhaft, R.N., Siqueira, P.R., 2000. Vertical structure of vegetated land surfaces from interferometric and polarimetric radar. Radio Sci. 35 (1), 141–177.
Treuhaft, R.N., Madsen, S.N., Moghaddam, M., Zyl, J.J., 1996. Vegetation characteristics and underlying topography from interferometric radar. Radio Sci. 31 (6), 1449–1485.
Treuhaft, R.N., Chapman, B.D., Dos Santos, J.R., Gonçalves, F.G., Dutra, L.V., Graca, P.M.L.A., Drake, J.B., 2009. Vegetation profiles in tropical forests from multibaseline interferometric synthetic aperture radar, field, and LiDAR measurements. J. Geophys. Res. D: Atmos. 114 (D23).
Treuhaft, R., Gonçalves, F., dos Santos, J.R., Palace, M., Keller, M., Madsen, S., Sullivan, F., Graca, P., 2014. Exploring vegetation profiles from TanDEM-X phase, lidar, and field measurements in tropical forests. In: EUSAR 2014; 10th European Conference on Synthetic Aperture Radar; Proceedings of (pp. 1–3). VDE.
Treuhaft, R., Gonçalves, F., dos Santos, J.R., Keller, M., Palace, M., Madsen, S.N., Sullivan, F., Graça, P.M., 2015. Tropical-forest biomass estimation at X-band from the space-borne TanDEM-X interferometer. IEEE Geosci. Remote Sens. Lett. 12 (2), 239–243.
Treuhaft, R., Lei, Y., Gonçalves, F., Keller, M., Santos, J.R.D., Neumann, M., Almeida, A., 2017. Tropical-forest structure and biomass dynamics from TanDEM-X radar interferometry. Forests 8 (8), 277.
Zebker, H.A., Villasenor, J., 1992. Decorrelation in interferometric radar echoes. IEEE Trans. Geosci. Rem. Sens. 30 (5), 950–959.